



HAL
open science

Multilayered models for determining the Young's modulus of thin films by means of Impulse Excitation Technique

Elia Zgheib, Akram Alhussein, Mohamed Fares Slim, Khaled Khalil, Manuel François

► To cite this version:

Elia Zgheib, Akram Alhussein, Mohamed Fares Slim, Khaled Khalil, Manuel François. Multilayered models for determining the Young's modulus of thin films by means of Impulse Excitation Technique. *Mechanics of Materials*, 2019, 137, pp.103143. 10.1016/j.mechmat.2019.103143 . hal-02279590

HAL Id: hal-02279590

<https://utt.hal.science/hal-02279590>

Submitted on 20 Jul 2022

HAL is a multi-disciplinary open access archive for the deposit and dissemination of scientific research documents, whether they are published or not. The documents may come from teaching and research institutions in France or abroad, or from public or private research centers.

L'archive ouverte pluridisciplinaire **HAL**, est destinée au dépôt et à la diffusion de documents scientifiques de niveau recherche, publiés ou non, émanant des établissements d'enseignement et de recherche français ou étrangers, des laboratoires publics ou privés.



Distributed under a Creative Commons Attribution - NonCommercial 4.0 International License

Multilayered models for determining the Young's modulus of thin films by means of Impulse Excitation Technique

Elia Zgheib ^{a,c,*}, Akram Alhussein ^a, Mohamed Fares Slim ^b, Khaled Khalil ^c, Manuel François ^b

^a ICD-LASMIS, Université de Technologie de Troyes, UMR 6281, CNRS, Antenne de Nogent, Pôle Technologique Sud-Champagne, 52800, Nogent, France.

^b ICD-LASMIS, Université de Technologie de Troyes, UMR 6281, CNRS, 12 Rue Marie Curie, CS 42060, 10004, Troyes, France.

^c Lebanese University, Faculty of Engineering, CRSI, MGC, Equipe MMC, Tripoli, Lebanon.

* Corresponding author: Elia Zgheib, elia.zgheib@utt.fr; zgheibelial@gmail.com; Tel.: +33-351-591-328

Abstract

This work presents a methodology to determine the Young's modulus of an individual coating in a multilayered system by means of the Impulse Excitation Technique (IET). In this technique, the composite beam is excited by an impulse and the frequencies of the first four bending modes are extracted. They are used in a one-dimensional model to obtain the Young's modulus of the coating. Based on two different theories: the Flexural Rigidity of a Composite Beam (FRCB) and the Classical Laminated Beam Theory (CLBT), different models proposed in the literature for bilayer beams have been extended to describe a beam composed of N dissimilar layers. Moreover, an enhanced model was developed based on the laminated theory. It takes into account the shift of the neutral axis after each deposited film, which makes it applicable for any film thickness. The reliability of the proposed model is investigated by comparing its predicted frequency to those of existing models for bilayers. It is also compared to finite element analysis of beams composed of two and three dissimilar layers. A metrological study was performed to quantify the most influencing factors on the global uncertainty. The methodology was applied to beams composed of three layers ($N=3$) with titanium and niobium thin films deposited by DC magnetron sputtering. The most accurate models are applied to obtain the Young's modulus of Ti and Nb films in the Ti/Nb/(AISI 316 or Glass) multilayer beam. The films microstructure and morphology were analyzed by X-ray diffraction and scanning electron microscopy.

Keywords: elasticity constants, multilayers, dynamical resonant method, coatings, physical vapor deposition, uncertainty.

1. Introduction

Thin film deposition is a common technology used to enhance surface properties. The films are elaborated in various ways to protect materials from different types of damage [1, 2] and to obtain functional surfaces. Numerous coating types have proven to be useful in a wide range of applications [3-6]. These various types of coatings can be used individually or in combination (multiple layers) depending on the requirements of the operating environment [7-10]. Multilayer structures containing metals, polymers and ceramics are widely used for modern technologies. Over the last twenty years, the investigation into the mechanical behavior of multilayer metallic thin films has attracted the attention of many researchers [11, 12]. For reliable and safe operation, knowledge of the elastic behavior of each individual layer and of the multilayers as a whole is of particular importance. The rigidity of these coatings has an important role to prevent cracks and structural failure. For example, if the rigidity of the coating does not correspond to the flexural stiffness of the base material, shear cracking can be produced [13].

Elasticity constants are the main parameters that affect the response of a film to mechanical stresses. Young's modulus is one of these important parameters describing the elastic deformation of materials. Even if this property is particularly difficult to determine for thin films, the Young's modulus of a coating is crucial in terms of load carrying capacity [14]. Many static and dynamic techniques were developed to determine the elastic constants of bulk and coated materials [15-18]. In the following, we will focus on the determination of the coating Young's modulus using a vibrational approach which is an accurate method to determine the mechanical behavior of materials. The Euler-Bernoulli bending beam theory was initially used to develop mathematical relations without taking into account the effects of shear and rotation. Subsequently, Timoshenko's equation was simplified to consider both effects by adding some correction factors [19]. These factors are determined as a function of the sample geometry and different vibration modes. After 1999, these improved equations have led to the formulation of the standardized ASTM-E1876 test method. The Impulse Excitation Technique (IET) is one of the vibrational techniques used to determine elastic modulus [11, 15, 20-22]. It is nondestructive and one of the less intrusive techniques, used with high precision to measure the elasticity constants of a wide range of materials such as metals, composites, ceramics, etc. [16, 19, 23] and especially coatings [21, 24, 25]. The principle of this vibrational test is to correlate the resonant frequencies of the tested specimen with its mechanical properties through a suitable model.

Using vibrational beam theory, several authors have developed a composite model (substrate + coating) for measuring the elastic modulus of a thin film. Berry et al. [26] were the first who used the IET to measure the Young's modulus of a composite system (substrate + film). The test relies on a two-step fundamental resonance frequency measurement of the sample: one measurement before deposition for the substrate and another one after deposition for the whole beam. After Berry et al., many researchers have used IET to test samples of various films with different thicknesses and elaboration techniques. For instance, Kim et al. [27] have used IET to test titanium (Ti)-coated silicon (Si) wafer specimens with different geometries, produced by radio frequency (RF) magnetron sputtering. They have shown that

the IET gives accurate results compared to a static method based on beam bending under a dead weight. Peraud et al. [28] have measured the Young's modulus of 2.2 μm thin silicon carbide (SiC) and of 2.5 μm thin nickel-titanium alloy (NiTi) manufactured by the Dynamic Ion Mixing (DIM) method. They have shown that IET allows us to determine the Young's modulus of very thin coatings. Cho et al. [29] have evaluated the Young's modulus of different metallic films: Ni, Co, Cr and Ti thin films deposited by RF magnetron sputtering with different thicknesses on Si wafers. In terms of film thickness variation, they found that the Young's modulus of Ni films decreased as the thickness of the film increased. For Cr and Co films, they did not find any significant difference. Etienne et al. [30] have measured the Young's modulus of titanium nitride (TiN) of 0.2 μm of thickness elaborated by ion implantation. Bellan et al. [15] have evaluated the elasticity constants of 35 μm thick SiC and 95 μm thick Pyrolytic Carbon (PyC) films elaborated by Chemical Vapor Deposition (CVD). They have shown that IET gives good and accurate results. The crystalline thin films are also used in the nanometric range such as in nano and microelectronic devices [7-10]. Hoy-Benítez et al. [25] have tested bilayer beams in a cantilever configuration and they measured the Young's modulus of gold (Au) films of 100 nm thickness deposited on polysulfone (PSF) substrates of 130 μm thickness. They found similar results to those reported in the literature.

For multilayer coatings, Cho et al. [29] have developed a model, based on the Flexural Rigidity of a Composite Beam (FRCB), to determine the film Young's modulus of a bi-coated substrate. They applied this model to Cr/Ti bilayer thin films manufactured by RF magnetron with different sputtering times deposited on Si wafers. They suggested that the Young's moduli of multilayer films might be obtained by repeatedly using a two-layer composite model. Recently, López-Puerto et al. [11] have developed a model based on the classical laminated beam theory (CLBT) and they applied it to obtain the elastic modulus of 200 nm aluminum (Al) and 250 nm thick Au films in an Al/Au/Kapton (125 μm) multilayer. After analyzing their model, they found that it provides great accuracy for the prediction of natural frequency in multilayered systems composed of thin films of less than 250 nm deposited on a thicker substrate.

The problem of determining the natural frequency of a multilayer as a function of the elasticity constants of thin films becomes complex for more than two layers but few analytical solutions exist for this situation requiring the use of advanced laminated theories [31, 32]. Many studies have been made based on this laminated theory [33-37] however; their solutions present a lack of a closed-form analytical expression due to mathematical complexity. Therefore, a one-dimensional solution seems to be inexistent to predict the resonant frequencies of multilayers as a function of elastic modulus for any case of coating-to-substrate thickness ratio at different flexural modes. Also, concerning the vibrational mode, a lack of information concerning the determination of Young's modulus using different modes measured by IET provides the motivation to carry out a thorough study and to develop new models which allow the determination of elastic modulus values.

The aim of this work is to develop new models able to determine the elasticity modulus of " N " arbitrary films in a multi-coated structure. It presents a vibrational approach

to determine the i^{th} ($i > 0$) harmonic resonant frequency as a function of the elasticity constants. The developed models take into account the shift of the neutral axis after deposition, which is essential in the case of layers with different elastic properties. They also take into account the effect of layering, the sources of error and the uncertainty of measurement. An investigation of the measurement accuracy will enable us to extract the true values of frequencies leading to the Young's modulus of coatings.

Firstly, a review of all the models developed in the literature to determine the Young's modulus of coatings and the theoretical background of the IET is presented. Secondly, an enhanced analytical formulation based on the classical laminated beam theory is developed to determine the macroscopic Young's modulus of " N " films ($N > 0$). It takes into account the shift of the neutral axis after deposition, which is an important factor affecting the solution, as was recently shown [38, 39]. An extension to multilayer structure is developed using the analytical models. The results were compared with the Finite Element Model (FEM) in order to validate the developed models. Finally, the models were validated experimentally and were applied to Ti and Nb films deposited by pulsed-DC magnetron sputtering on different substrates.

2. Vibrational modeling

2.1. Homogeneous beam

In the analysis of the flexural vibrations of a uniform isotropic beam, the Euler-Bernoulli equation is considered, neglecting the effects of shear and rotational inertia. The motion of a beam with length L , width b and thickness h , cross-sectional area S , mass density ρ , elastic modulus E , and second moment of area I_y subjected to flexural (z) vibrations can be described by the following differential equation, where w is the displacement along z [37]:

$$\rho S \frac{\partial^2 w(x, t)}{\partial t^2} + \frac{\partial^2}{\partial x^2} \left(EI_y \frac{\partial^2 w(x, t)}{\partial x^2} \right) = 0 \quad (1)$$

This differential equation can be solved analytically to determine the modal shapes and the natural frequencies of the vibration modes. In the present study, a free-free (FF) beam with a rectangular cross-section is used and the characteristic equation corresponding to these boundary conditions is:

$$\cos X_n \cosh X_n - 1 = 0 \quad (2)$$

By solving Eq. (2), the non-dimensional Eigen frequencies X_n for the first four mode shapes were determined. Then, the resonant frequencies can be determined from the following equation [37]:

$$f_0^{(n)} = \frac{X_n^2}{2\pi L^2} \sqrt{\frac{E_0 I_0}{\rho_0 S_0}} \quad (3)$$

Where the subscript “0” corresponds to the substrate. By inverting Eq. (3), the corresponding Young’s modulus can be determined from the following expression:

$$E_0 = \left(\frac{2\pi L^2}{X_n^2} \right)^2 \frac{\rho_0 S_0}{I_0} \left(f_0^{(n)} \right)^2 \quad (4)$$

The IET can be used to determine the Young’s modulus, in the case of FF beam with a rectangular cross-section, according to the following equation [40]:

$$E_0 = k_1 \rho_0 \frac{L^4}{h_0^2} T_f \left(f_0^{(1)} \right)^2 \quad (5)$$

Where $k_1 \approx 0.9465$. T_f is a geometrical correction factor introduced to take into account the shear and rotary inertia effects [40]:

$$T_f = 1 + 6.585(1 + 0.0752\nu_0 + 0.8109\nu_0^2) \left(\frac{h_0}{L} \right)^2 - 0.868 \left(\frac{h_0}{L} \right)^4 - \left[\frac{8.34(1 + 0.2023\nu_0 + 2.173\nu_0^2) \left(\frac{h_0}{L} \right)^4}{(1 + 6.338(1 + 0.1408\nu_0 + 1.536\nu_0^2) \left(\frac{h_0}{L} \right)^2)} \right] \quad (6)$$

Where ν_0 is the substrate Poisson’s ratio. For the case of $h_s / L \leq 0.05$, Eq. (6) can be simplified into the following expression:

$$T_f = 1 + k_2 \left(\frac{h_0}{L} \right)^2 \quad (7)$$

Where $k_2 \approx 6.585$

2.2. Composite beam structure

The composite beam considered herein is a FF beam of length L , width b with rectangular cross-sectional area and total thickness h_t constituted of a substrate and N dissimilar coatings (Fig. 1a); each one indicated by the index k ($k=1, \dots, N$) as shown in Fig. 1b. The vibration measurements of the resonance frequencies are conducted sequentially, first for the substrate, then after each deposited film. This order of measurements requires the determination of the elastic modulus of the k^{th} film ($k > 0$) before depositing the following one $(k+1)^{th}$. Using these frequencies, the Young’s modulus of each individual film can be determined through analytical models that are proposed in the literature based on two different theories: the flexural rigidity of a composite beam (FRCB) and the classical laminated beam theory (CLBT).

a)

b)

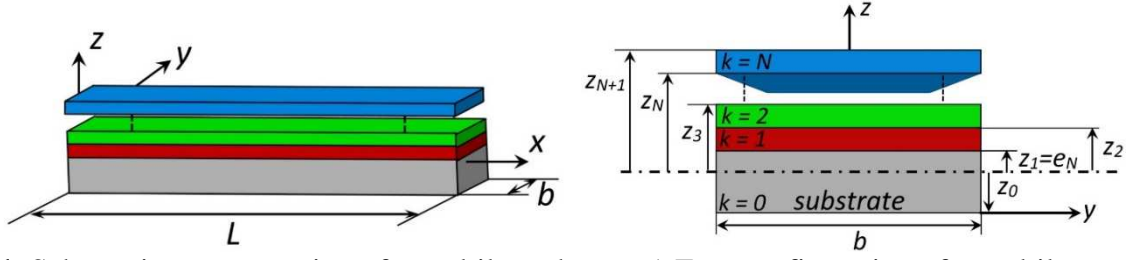


Fig. 1. Schematic representation of a multilayer beam. a) Free configuration of a multilayer beam. b) The z -coordinates of each layer in a cross-sectional view.

2.2.1. Models based on FRCB

The FRCB theory assumes that the coatings are perfectly homogeneous and adherent to the substrate and the expression of the “ n ” resonant frequencies of the composite beam can be determined, using the Euler-Bernoulli solution (Eq. 3) as follows:

$$f_N^{(n)} = \frac{X_n^2}{2\pi L^2} \sqrt{\frac{E_t I_t}{\rho_t S_t}} \quad (8)$$

Where $E_t I_t$ is the flexural rigidity of the entire composite beam expressed as the sum of the flexural rigidity of each layer (Eq. 9). Moreover, the product $\rho_t S_t$ is expressed as the summation of the corresponding product of each layer (Eq. 10) [41].

$$E_t I_t = \sum_{k=0}^N E_k I_k \quad (9)$$

$$\rho_t S_t = \sum_{k=0}^N \rho_k S_k \quad (10)$$

The subscripts “0”, “ k ”, “ t ” and “ N ” correspond to substrate, k^{th} film, whole beam and the total number of coatings, respectively.

Many models were developed [20, 22, 23, 26] with analytical expressions for a FF composite beam (substrate + coating) with a rectangular cross-sectional area to determine the Young’s modulus of a single layer coating ($N=1$). Some of these models [22, 26] assumed that the neutral axis remains fixed after deposition (it always corresponds to the mid-plane of the substrate cross-section). With this assumption, no shifting of the neutral surface is considered and a systematic error increases with the film thickness. Contrariwise, Pautrot’s model [20, 22, 23] was developed in order to take into account the shift of the neutral axis after deposition (Fig. 2a). This shift can be determined using the equilibrium of the axial forces [41] generated during pure bending (Fig. 2b).

a)

b)

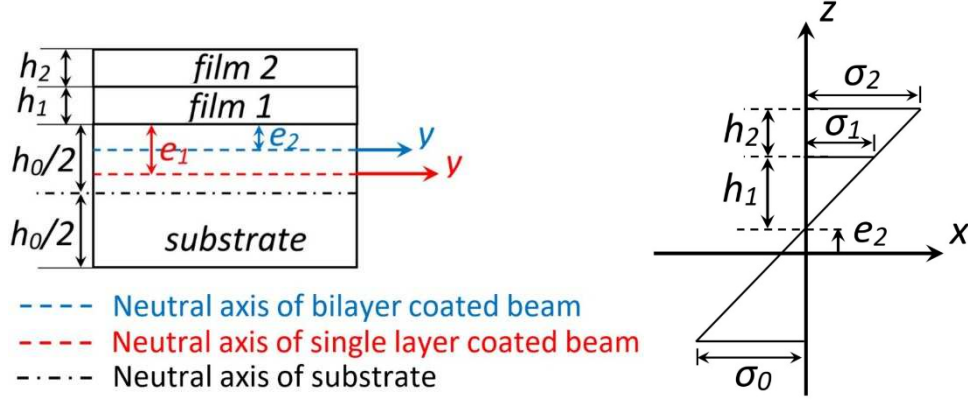


Fig. 2. Schematic representation of the shift of the neutral axis: a) cross-sectional view, b) stress distribution in three-layer composite beam.

Developing Eq. (8) by taking into consideration the shift in the expressions of second moments of area of both substrate and coating of Eq. (9), we obtain the analytical expression developed by Pautrot et al., expressing the ratio of the frequencies of the substrate and the coated substrate [20, 22, 23]:

$$(R_{f1})^2 = \frac{(R_{E1}R_{h1}^3 + 1)(R_{E1}R_{h1} + 1) + 3R_{E1}R_{h1}(R_{h1} + 1)^2}{(R_{\rho1}R_{h1} + 1)(R_{E1}R_{h1} + 1)} \quad (11)$$

Where:

$$R_{h1} = \frac{h_1}{h_0} \quad (12)$$

$$R_{\rho1} = \frac{\rho_1}{\rho_0} \quad (13)$$

$$R_{E1} = \frac{E_1}{E_0} \quad (14)$$

$$R_{f1} = \frac{f_1}{f_0} \quad (15)$$

Then, by inverting Eq. (11), the Young's modulus of the coating can be calculated using the following expression:

$$\begin{aligned}
 E_1 = \frac{E_0}{2R_{h1}^4} & \left[(R_{h1} + R_{\rho1}R_{h1}^2)(R_{f1})^2 - 4R_{h1}^3 - 6R_{h1}^2 - 4R_{h1} \right. \\
 & + \left(4R_{h1}^4 \left[(1 + R_{h1}R_{\rho1})(R_{f1})^2 - 1 \right] \right. \\
 & \left. \left. + \left[4R_{h1}^3 + 6R_{h1}^2 + 4R_{h1} - (R_{h1} + R_{\rho1}R_{h1}^2)(R_{f1})^2 \right]^2 \right)^{0.5} \right] \quad (16)
 \end{aligned}$$

Whiting et al. [23] have provided a simplified expression for a more direct calculation of the film elastic modulus with further simplification related to the thin film geometry as:

$$E_1 = \frac{E_0}{3} \left[\frac{2R_{f1} + R_{\rho1}R_{h1} - 2}{R_{h1}} \right] \quad (17)$$

Where $R_{hl} \ll 1$ and the terms containing powers of R_{hl} greater than one may be neglected. The more general equation, Eq. (16), will be employed in this work to increase the accuracy. Note that all the models discussed above, for the resonant frequency of a bilayer beam (substrate + coating), are based on FRCB of isotropic materials and they neglect material anisotropy and damping contributions such as material viscoelasticity or other hysteretic effects [42].

2.2.2. Model based on CLBT

In this section, a simplified one-dimensional (1D) model based on CLBT is used to determine the Young's modulus of an individual thin film in a multilayer beam structure. It fulfills Kirchhoff's law [43] and it is applicable for one, two and multiple layers [31, 32]. This theory assumes that the beam is symmetrical about the mid-surface of the composite beam with respect to the z -axis (Fig. 3) and neglects the effect of shear deformations with no coupling between bending and extension [25, 31]. These two assumptions are not respected in most cases where the film is deposited on one side of the substrate. However, it can be used as an approximation in the case of an asymmetric beam of several thin films deposited on a thicker substrate. Obviously, the higher the ratio of Young's moduli and the thicknesses ratio, the higher the error associated with this model is [11, 24].

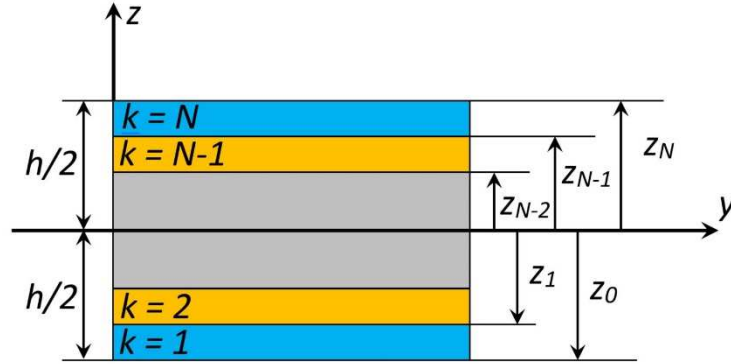


Fig. 3. Schematic view of a symmetrical laminated beam.

In the case of a laminated beam, the bending stiffness matrix D_{ij} (3x3) can be expressed as follows [43]:

$$D_{ij} = \int_{z_{k-1}}^{z_k} \bar{Q}_{ij}^{(k)} z^2 dz = \frac{1}{3} \sum_{k=1}^{N+1} \bar{Q}_{ij}^{(k)} (z_k^3 - z_{k-1}^3) \quad \begin{cases} i, j = 1, 2 \text{ or } 6 \\ k = 1, \dots, N+1 \end{cases} \quad (18)$$

Where z_k is the coordinate of the k^{th} layer and $\bar{Q}_{ij}^{(k)}$ are the transformed reduced stiffness elements, the function of the reduced stiffness including information on elastic modulus, Poisson's ratio, and the orientation (Θ) of the k^{th} layer [11,43].

Working with the x-y axes as principal axes for both substrate and film leads to obtain a zero-layer orientation ($\Theta = 0$) [11]. For isotropic substrate and film materials, the stiffness elements become:

$$\bar{Q}_{11}^{(k)} = \bar{Q}_{22}^{(k)} = Q_{11}^{(k)} = Q_{22}^{(k)} = \frac{E_k}{1 - (\nu_k)^2} \quad (19)$$

$$\bar{Q}_{12}^{(k)} = Q_{12}^{(k)} = \frac{\nu_k E_k}{1 - (\nu_k)^2} \quad (20)$$

$$\bar{Q}_{16}^{(k)} = \bar{Q}_{26}^{(k)} = 0 \quad (21)$$

$$\bar{Q}_{66}^{(k)} = Q_{66}^{(k)} = \frac{E_k}{2(1 + \nu_k)} \quad (22)$$

Where:

E_k : Elastic modulus of the k^{th} layer.

ν_k : Poisson's ratio of the k^{th} layer.

The flexural moment per unit width M_y , producing transverse deflections w can be expressed in terms of the curvature as [43]:

$$M_y = -\frac{1}{d_{11}^N} \frac{\partial^2 w}{\partial x^2} \quad (23)$$

Where d_{11} is the (1,1) element of the bending matrix $[d]=[D]^{-1}$. For a symmetrical laminated beam, d_{11} can be expressed as:

$$d_{11}^{(N)} = \frac{D_{22}}{\det[D]} \quad (24)$$

$$\det[D] = D_{11}D_{22} - D_{12}^2 \quad (25)$$

Where $\det [D]$ is the determinant of the matrix D_{ij} .

The vibrating laminated beam subjected to a flexural moment M_y with transverse displacements w can be expressed, according to CLBT, by the following equation [11]:

$$\frac{\partial^2 M_y}{\partial x^2} = \rho_{eff}^{(N)} \frac{\partial^2 w}{\partial t^2} \quad (26)$$

Where ρ_{eff} is the weighted area density (in kg/m^2) expressed as:

$$\rho_{eff}^{(N)} = \int_{-(\sum_{k=0}^N h_k)/2}^{(\sum_{k=0}^N h_k)/2} \rho_k dz = \sum_{k=0}^N \rho_k h_k \quad (27)$$

By substituting Eq. (23) into Eq. (26), the following differential equation of the transverse vibration of a symmetric laminated beam is obtained:

$$\frac{1}{d_{11}^{(N)} \rho_{eff}^{(N)}} \frac{\partial^4 w}{\partial x^4} + \frac{\partial^2 w}{\partial t^2} = 0 \quad (28)$$

Where the term d_{11} contains the properties of each layer (Young's modulus, Poisson's ratio and thickness). Notice that Eq. (28) has the same form as Eq. (1) for a homogeneous isotropic beam when carrying out the following transformations:

$$E_0 \rightarrow \frac{12}{h_0^3 d_{11}^{(N)}} \quad (29)$$

$$\rho_0 \rightarrow \frac{\rho_{eff}^{(N)}}{h_0} \quad (30)$$

By substituting Eqs. (29) and (30) into Eq. (3), the resonant frequencies of a laminated beam can be expressed as:

$$f_N^{(n)} = \frac{X_n^2}{2\pi L^2} \sqrt{\frac{1}{d_{11}^{(N)} \rho_{eff}^{(N)}}} \quad (31)$$

The frequency ratio becomes:

$$(R_{f(N)})^2 = \frac{12\rho_0}{E_0 h_0^2} \left(\frac{1}{d_{11}^{(N)} \rho_{eff}^{(N)}} \right) \quad (32)$$

Much research has already been performed using the CLBT model in order to determine the elastic modulus of thin film [11, 24]. By comparing their model to a finite element model (FEM), López-Puerto et al. [11] found that the CLBT model is limited to a film thickness of 250 nm ($R_{hl} < 0.002$). In our previous study [24], we found that the optimum error zone associated with the CLBT model is centered at Young's modulus ratio equal to 1. This is due to the assumption of symmetry on which is based the CLBT model. We also found that Pautrot's model presents the closest results to those of the finite element model. The next two sections (2.3 and 2.4) present two developed models based on the theories presented above. These models describe the behavior of multilayer beams in flexural vibrations.

2.3. Extended Pautrot's model (Ext-PM)

As Pautrot's model was the best used to determine the Young's modulus of single layer coatings, an extension is applied to it, where the neutral axis will shift after each layer deposited. This shift can be generalized for any number "N" of isotropic layers using a generalized equation of equilibrium of the axial forces as follows:

$$\sum_{k=0}^N \iint \sigma_k dS_k = \int_{-h_0+e_N}^{e_N} E_0 z dz + \sum_{k=1}^N \int_{Z_1}^{Z_2} E_k z dz = 0 \quad (33)$$

With:

$$Z_1 = e_N + \delta_k \sum_{j=1}^{k-1} h_j \quad \delta_k = \begin{cases} 0 & \text{if } k = 1 \\ 1 & \text{if } k \neq 1 \end{cases} \quad (k = 1, \dots, N) \quad (34)$$

$$Z_2 = Z_1 + h_k$$

By integrating Eq. (33) and applying the static equilibrium of a beam in pure bending, the generalized shift e_N becomes:

$$e_N = \frac{E_0 h_0^2 - \sum_{i=1}^N E_i h_i [h_i + 2\delta_i \sum_{j=2}^i h_{j-1}]}{2 \sum_{i=0}^N E_i h_i} \quad (35)$$

Developing Eq. (8) by taking into consideration the shift (e_2) of a bi-coated beam ($N=2$) in the expressions of second moments of inertia of both substrate and coating of Eq. (9), we obtain the new analytical expression developed herein, expressing the ratio of the frequencies of the substrate and the bi-coated substrate:

$$(R_{f2})^2 = \frac{1 + A (R_{E1})^2 + B (R_{E2})^2 + 2C R_{E1} R_{h1} + 2D R_{E2} R_{h2}}{(1 + R_{h1} R_{\rho1} + R_{h2} R_{\rho2})(1 + R_{E1} R_{h1} + R_{E2} R_{h2})} \quad (36)$$

Where:

$$R_{h2} = \frac{h_2}{h_0} \quad (37)$$

$$R_{\rho2} = \frac{\rho_2}{\rho_0} \quad (38)$$

$$R_{E2} = \frac{E_2}{E_0} \quad (39)$$

$$R_{f2} = \frac{f_2}{f_0} \quad (40)$$

$$A = R_{h1}^4 \quad (41)$$

$$B = R_{h2}^4 \quad (42)$$

$$C = 2 + 6R_{h1}(R_{h1} + R_{h2} + 1) + R_{h2}(3 + 2R_{h2}) \quad (43)$$

$$D = R_{E2} R_{h2} (2R_{h1}^2 + 3R_{h1} R_{h2} + 2R_{h2}^2) + 2R_{h1}^2 + 3R_{h1} + 2 \quad (44)$$

Knowing the thicknesses and, mass densities of the substrate and of the two films, the Young's modulus of the substrate and of the first film, and by inverting Eq. (36), the Young's modulus of the second film is determined using the following equation:

$$E_2 = \frac{-b_1 + \sqrt{b_1^2 - 4a_1 c_1}}{2a_1} \quad (45)$$

Where:

$$a_1 = R_{h2}^4 \quad (46)$$

$$\begin{aligned}
b_1 = & 4R_{h2}^3(1 + R_{E1}R_{h1}) + R_{h2}^2 \left[6 - R_{\rho2}(R_{f2})^2 + 6R_{h1}(2 + R_{E1}R_{h1}) \right] \\
& + R_{h2} \left[4 - (R_{f2})^2 + 4R_{h1}^2(3 + R_{E1}R_{h1}) \right] \\
& + R_{h1} \left[12 - R_{\rho1}(R_{f2})^2 \right]
\end{aligned} \tag{47}$$

$$\begin{aligned}
c_1 = & 1 - (1 + R_{E1}R_{h1})(1 + R_{\rho1}R_{h1} + R_{\rho2}R_{h2})(R_{f2})^2 \\
& + R_{E1}R_{h1}(4 + 6R_{h1} + 4R_{h1}^2 + R_{E1}R_{h1}^3)
\end{aligned} \tag{48}$$

2.4. Enhancement of the CLBT model (Dev-CLBT)

As in the case of single layer coated beams, the CLBT model can be used to determine the Young's modulus of the k^{th} layer (E_k) if the elastic modulus of the $(k-1)^{th}$, $(k-2)^{th}$, ..., 1^{st} layers are known. For instance, in a bi-coated isotropic beam structure, the 3x3 bending stiffness matrix D_{ij} is defined in Eq. (18) with $N=2$. An enhancement of the CLBT model is developed herein for “ N ” dissimilar layers; assuming that the neutral axis will shift after deposition using the shift of Eq. (35) and the new 3x3 bending stiffness matrix:

$$D'_{ij} = \int_{-h_0+e_N}^{e_N} \bar{Q}_{ij}^{(0)} z^2 dz + \sum_{k=1}^N \int_{Z_1}^{Z_2} \bar{Q}_{ij}^{(k)} z^2 dz \quad (i, j = 1, 2 \text{ or } 6) \tag{49}$$

Where Z_1, Z_2 are expressed in Eq. (34).

Inverting the new sub-matrix D'_{ij} of Eq. (49) for the case of a bi-coated ($N=2$) isotropic beam and applying the expression of d_{11} from Eq. (24), the new R_0, R_1 and R_2 functions of the thicknesses and the shift e_2 , are determined as:

$$\begin{aligned}
d_{11}^{(2)} &= \frac{\frac{E_0 R_0}{1 - \nu_0^2} + \frac{E_1 R_1}{1 - \nu_1^2} + \frac{E_2 R_2}{1 - \nu_2^2}}{\left[\frac{E_0 R_0}{1 - \nu_0^2} + \frac{E_1 R_1}{1 - \nu_1^2} + \frac{E_2 R_2}{1 - \nu_2^2} \right]^2 - \left[\frac{\nu_0 E_0 R_0}{1 - \nu_0^2} + \frac{\nu_1 E_1 R_1}{1 - \nu_1^2} + \frac{\nu_2 E_2 R_2}{1 - \nu_2^2} \right]^2}
\end{aligned} \tag{50}$$

With:

$$R_0 = \frac{h_0^3}{3} - e_2 h_0^2 + e_2^2 h_0 \tag{51}$$

$$R_1 = \frac{h_1^3}{3} + e_2 h_1^2 + e_2^2 h_1 \tag{52}$$

$$R_2 = \frac{h_2^3}{3} + (e_2 + h_1)(e_2 + h_1 + h_2)h_2 \tag{53}$$

The frequency ratio of a laminated beam is expressed using Eq. (32) with the new expressions of D'_{ij} and d_{11} from Eqs. (49) and (50), respectively. This expression is an implicit function. Therefore, in order to determine the solution, an iteration loop is applied using bisection method [44]. The unknown elastic modulus of the second film (E_2) is then found.

For bilayer coatings, López-Puerto et al. [11] proved that the solution depends on the stacking sequence selected (Au/Al/Kapton or Al/Au/Kapton) because of the lack of symmetry that can lead to larger errors (>1.3%) in the prediction of the frequency of a multi-coated beam using CLBT. Therefore, the developed models, based on the two different theories (FRCB and CLBT) will be examined by comparing them to a numerical model based on finite element analysis (FEA) in order to analyze quantitatively the difference between them. An outline of the analytical models proposed in the literature and the models developed in the present paper is presented in Table 1.

Table 1
Summary of the analytical models.

Model	Theory	Nb. of layers	Assumptions
Lopez [22]	FRCB	Bilayer	Isotropy
Berry [26]	FRCB	Bilayer	Simplification of Lopez's model
Pautrot [20, 22, 23]	FRCB	Bilayer	Isotropy & Shift
Whiting [23]	FRCB	Bilayer	Simplification of Pautrot's model
CLBT [11]	CLBT	Multilayer	Symmetry & Anisotropy
Extended Pautrot (Ext-PM)	FRCB	Multilayer	Isotropy & Shift
Developed (Dev-CLBT)	CLBT	Multilayer	Symmetry, Anisotropy & Shift

3. Experimental details

3.1. Thin film deposition

High purity (99.99%) titanium (Ti) and niobium (Nb) thin films were deposited on stainless steel AISI 316 (sample 1), glass (sample 2) substrates and silicon (Si) wafers by magnetron sputtering in DC pulsed mode. The substrates were ultrasonically cleaned in acetone and ethanol for 10 min. Before deposition, they were cleaned by an Argon plasma etching at 0.38 Pa and 200 W ($U_{bias}=21$ V) during 30 min to remove impurities and surface oxides that could alter the quality of the adhesion of the films. In this phase, the Ti and Nb targets were pre-sputtered for 15 min.

A DEPHIS4 Physical Vapor Deposition (PVD) machine was used with a 600 mm diameter cylindrical deposition chamber of 400 mm in height that was pumped down with a turbomolecular pump to less than 10^{-6} Pa before filling it with argon (Ar) gas. An argon flow rate of 50 sccm led to a constant working pressure of 0.2 Pa. The target-substrate distance was kept constant at 10 cm.

Using a DC-pulsed power supply, the intensity applied to the targets was 3 A of a 275 V discharge voltage (frequency = 50 kHz; time off = 4 μ s) for the first film of Ti and 228 V (frequency = 100 kHz; time off = 4 μ s) for the second film of Nb. The substrates were placed on a rotating holder (10 rpm) to ensure a perfect thickness homogeneity of the films. Under these conditions, the deposition of the first (Ti) and second (Nb) films was carried out with a deposition rate of 16.13 nm/min and 18.90 nm/min, respectively. The stainless steel (AISI 316) and glass substrates were used for IET and nanoindentation characterizations and Si (100) wafers for the Scanning Electron Microscopy (SEM) images.

3.2. Dimensions and Density

The coating has the same length and width as the substrate with different thicknesses. The dimensions of each substrate were measured ten times in ten different locations. The average dimensions and their uncertainties are represented in Table 2. Samples 1 and 2 correspond to Nb/Ti/AISI 316 and Nb/Ti/Glass configurations, respectively. The standard uncertainties on the measured dimensions were evaluated by a type A method by computing the standard deviation [45]. The mass of the substrate was measured using a Sartorius precision balance and then its density was calculated. The uncertainties on the substrate masses were evaluated following a type B procedure [45]. According to technical specifications of the precision balance used, the uncertainty is equal to 0.1 mg. After deposition, the mass of the composite beam was measured. The bilayer beam corresponds to the Ti film deposited on the substrate. The second film was deposited on the previous beam in order to obtain a three-layered beam. The corresponding values are presented in Table 3. The difference in mass measured before and after each deposited film corresponds to the mass of the film. Its density was estimated by considering the mass and the dimensions of the film.

Table 2
Average dimensions and measurement uncertainty.

		Length (mm)		Width (mm)		Thickness (mm)	
		L	$u(L)$	b	$u(b)$	h	$u(h)$
Sample 1	Substrate (AISI 316)	69.98	0.027	19.97	4.7×10^{-3}	0.505	2.6×10^{-3}
	Film 1 (Ti)	69.98	0.027	19.97	4.7×10^{-3}	4.84	0.013
	Film 2 (Nb)	69.98	0.027	19.97	4.7×10^{-3}	3.97	0.029
Sample 2	Substrate (Glass)	75.33	0.036	25.38	9.4×10^{-3}	1.016	8.1×10^{-3}
	Film 1 (Ti)	75.33	0.036	25.38	9.4×10^{-3}	4.84	0.013
	Film 2 (Nb)	75.33	0.036	25.38	9.4×10^{-3}	3.97	0.029

Table 3
Mass and density with the measurement uncertainty.

		Masse (g)	Density (kg/m^3)	
		m	ρ	$u(\rho)$
Sample 1	Substrate (AISI 316)	5.561	7879.70	40.75
	Film 1 (Ti)	0.031	4583.15	148.37
	Film 2 (Nb)	0.044	7930.68	189.36
Sample 2	Substrate (Glass)	4.774	2457.70	19.66
	Film 1 (Ti)	0.043	4646.90	108.82
	Film 2 (Nb)	0.063	8300.24	145.12

3.3. Morphology

Using a Hitachi S3500N SEM-FEG operated at 15 kV, the thickness of each bilayer film was measured ten times in ten different positions in order to determine the average thicknesses and their uncertainties (Table 2). Fig. 4 shows the fractured cross-sectional SEM image of Nb/Ti/Si multilayer sample. No significant variation appears in the film thickness. It can clearly be seen that the two films present a porous microstructure with a relatively columnar growth. This can be due to the change in energies of incident ions that are

transferred to adatoms during the deposition [46, 47]. The deposition rate and pressure [48, 49] affect these energies. Besides, the absence of bias (polarization) can also favor this columnar film growth [46].

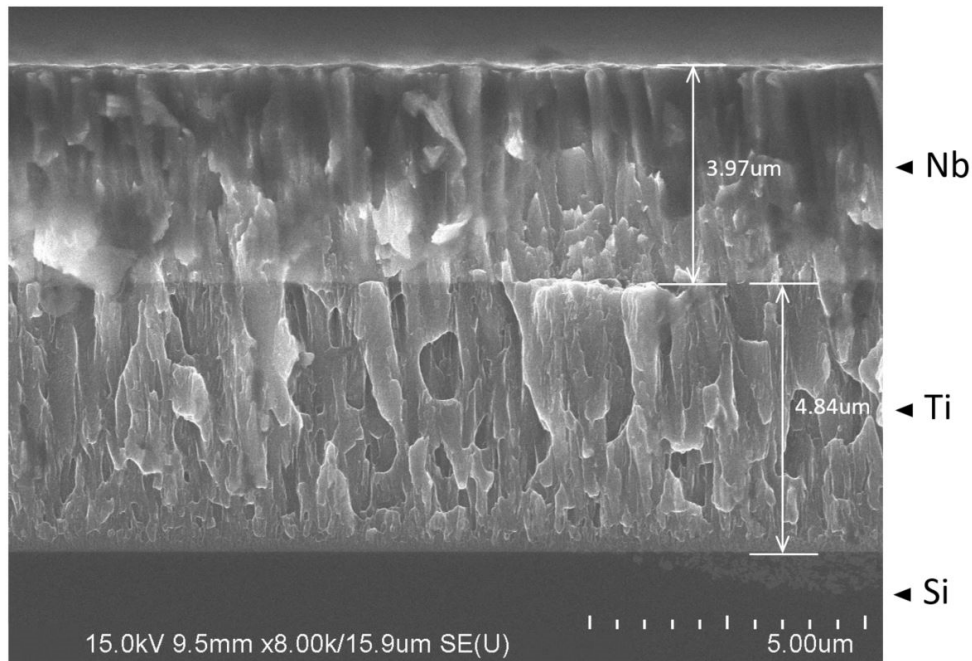


Fig. 4. Cross-sectional SEM image of the titanium and niobium films deposited on silicon substrate.

3.4. Characterizations

3.4.1. IET experiments

The Impulse Excitation Technique (IET) is used to measure the natural frequencies of a specimen impacted by a striker. A beam can be excited in longitudinal, flexural and torsional vibrational modes [40]. The sample is placed on a support with negligible interaction (nylon wires placed along the nodal lines of the considered mode) in order to adopt a free-free (FF) boundary condition. These conditions are the simplest to adopt because they represent the configuration with the least interaction between the support system and the specimen compared with the other configurations. An RFDA professional signal analysis system (Resonance Frequency and Damping Analysis) from IMCE Company (Genk, Belgium) was used to measure the resonant frequencies. It is equipped with an RFDA transducer, an acoustic microphone with a frequency range up to 100 kHz, a universal wire support, an automatic excitation unit and a computer system equipped with RFDA software. The microphone detects the mechanical vibrations produced during the excitation of the sample. The detected vibrations are transformed by a transducer into an electrical signal that determines the vibration amplitudes as a function of time. Using the Fast Fourier Transform (FFT), the amplitudes are transformed as a function of frequency defining the resonant frequencies of the sample at different vibration modes. The sample's support used is composed of wires located at the nodal points of the beam where the displacement is equal to

zero. More detailed explanations of the procedure can be found in the literature [40]. The measurement reliability can be characterized by its trueness and its accuracy, which were investigated in our previous paper [24].

The first four resonant frequencies of substrates (316L, Glass), bilayer (Ti/316L, Ti/Glass) and three-layer composite beams (Nb/Ti/316L, Nb/Ti/Glass) were measured. The vibration measurements were conducted sequentially, i.e., firstly, the resonant frequencies of the substrates were determined; then the titanium film was deposited on each substrate and the resonant frequencies of each bilayer beam were measured again; finally, the third layer (Nb) was deposited and the resonant frequencies of the three-layered beams were measured. As seen from Fig. 5, the frequency is shifted 2.58 Hz when the Ti film is deposited, and a new additional shift of 0.78 Hz is observed when the Nb film is deposited on the Ti/316L beam. These frequency shifts were used to calculate the substrate and films Young's moduli using the corresponding analytical model.

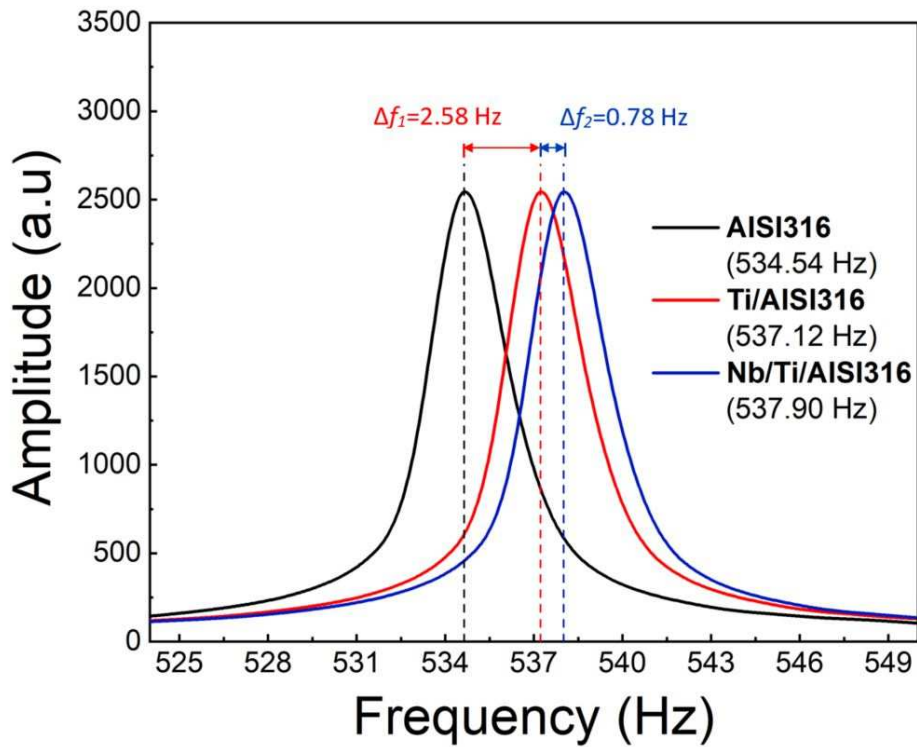


Fig. 5. The natural frequency of the substrate (AISI 316), one layer coated substrate (Ti/AISI 316) and the multilayer comprising three materials (Nb/Ti/AISI 316).

3.4.2. Nanoindentation

The contact reduced elasticity moduli of the films were also measured by nanoindentation (NI) tests using a TriboIndenter TI 980-Hysitron with continuous stiffness measurement (CSM) option. For the measurements, a Berkovich diamond tip was used with elasticity constants $E_{ind}=1140$ GPa and $\nu_{ind} = 0.07$. Before performing the measurements, the equipment was calibrated using a reference polycarbonate glass specimen.

The films' reduced moduli were determined by taking the average of ten indents and the uncertainty of measurements was determined from their standard deviation. The tests were

carried out under controlled load. In order to minimize the influence of the substrate or of previous layers, the indenter penetration depth was kept lower than 10 % of the coating thickness [50]. The corresponding penetration depth was found to be about 270 nm (8000 μ N) for titanium and 300 nm (8000 μ N) for niobium. The contact reduced modulus of the sample and the indenter can be expressed as [51-53]:

$$E_r^c = \frac{\sqrt{\pi} S}{2\beta \sqrt{A}} \quad (54)$$

Where β is a constant that depends on the geometry of the indenter, S is the contact stiffness and A is the projected contact area.

Thus, the Young's modulus of the indented material can be calculated from the contact reduced stiffness and the elastic properties of the tip as [51-54]:

$$E = (1 - \nu^2) \left[\frac{1}{E_r^c} - \frac{1 - \nu_{ind}^2}{E_{ind}} \right]^{-1} \quad (55)$$

Where E_r^c is the contact reduced modulus, E_{ind} and ν_{ind} are respectively the Young's modulus and the Poisson's ratio of the tip, E and ν are respectively the Young's modulus and Poisson's ratio of the indented material. More detailed explanations of the procedure can be found in the literature [51-54].

3.4.3. X-ray Diffraction

X-ray diffraction (XRD) was employed to identify the crystallographic structure of the films using a Bruker D8 Advance diffractometer equipped with a $\text{CuK}\alpha$ ($\lambda=0.15418$ nm) radiation operated at 40 kV and 40 mA. Different spectra were acquired at different inclination angles Ψ . The data, in the range of 2θ between 20° and 150° , were collected. Analysis of the diffraction patterns was performed using DIFFRAC.EVA software.

4. Numerical simulation

Finite element analysis (FEA) was carried out using the commercial finite element code ABAQUS [55] in order to determine the frequencies in the flexural mode of the naked substrate, the bilayer and the three-layered beams. Fig. 6 represents the first four vibration modes of a FF multilayered beam. The beam has a length L of 70 mm, width b of 20 mm and thickness h_0 of 1 mm with a rectangular cross-section. Two different finite element models were constructed by bonding the coatings on the substrate already created through one of two different functions: tie or partition; that give no significant differences in the “ n ” modes of frequency extracted. The first model presents a single layer coated beam with a film thickness h_1 that was varied from 0 to 1 mm. The second one represents a bi-coated beam with a first film thicknesses h_1 of 4 μ m ($R_{h1} = 4 \times 10^{-3}$) and 100 μ m ($R_{h1} = 0.1$) and a second film with a thickness h_2 that varied from 0 to 0.55 mm.

a)

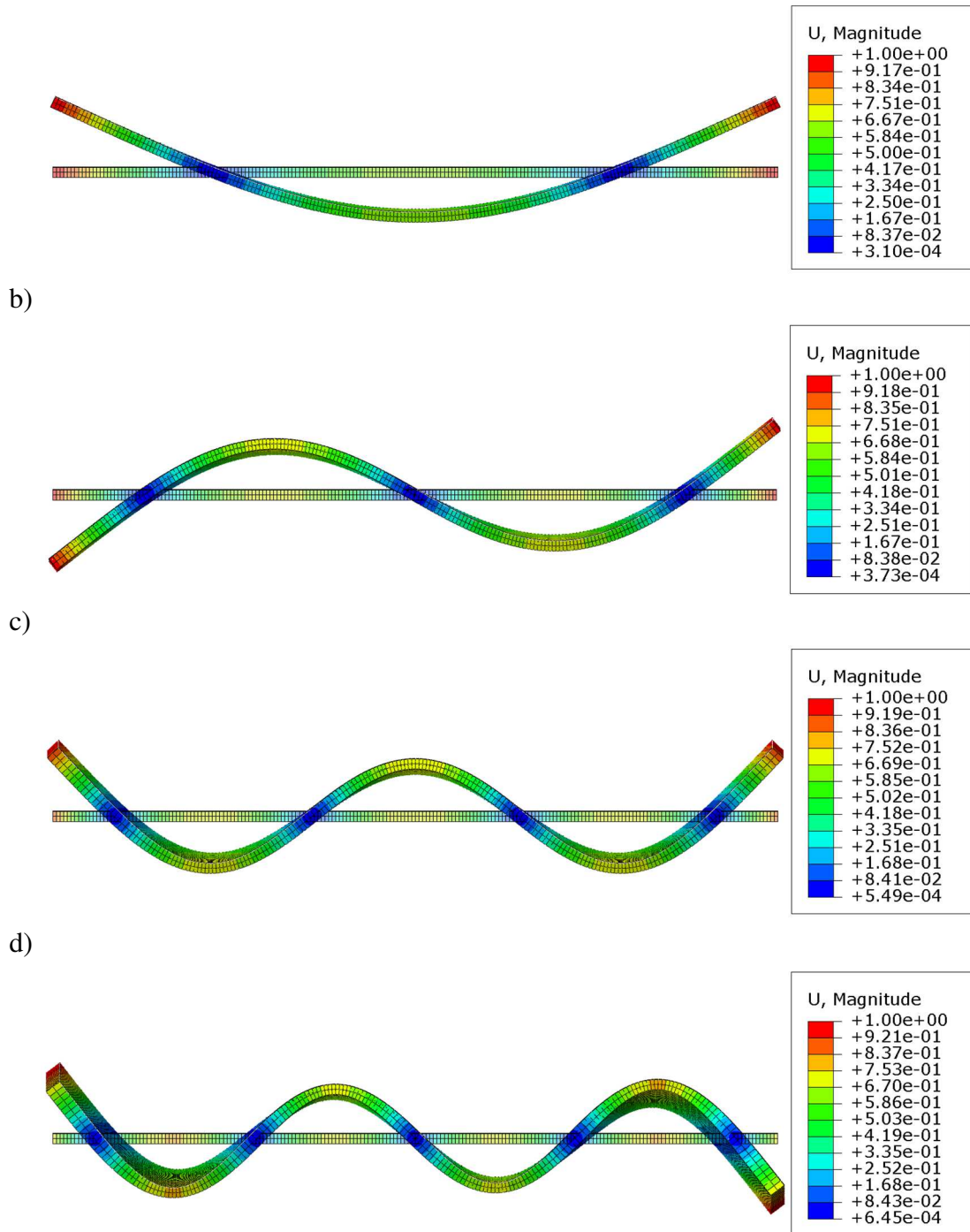


Fig. 6. Deformed flexural vibrating beam: a) mode I, b) mode II, c) mode III and d) mode IV. The colors indicate the vertical displacement (mm).

To mesh the structure, C3D20 quadratic element was used since it presents excellent behavior for linear elastic calculations. A mesh convergence study of the first four frequency modes was performed to determine the mesh density at which the values of the first four resonant frequencies converge. By varying the number of elements in all three directions, the element size of $0.35 \times 0.27 \times 0.5 \text{ mm}^3$ was chosen for the substrate that led to invariant frequency values even with the smallest elements. Considering the beam dimensions mentioned in the first paragraph, it gives 30,000 elements: 200 in the length direction, 75 in

the width and 2 in the thickness. For a multilayer beam with $R_{hl} > 0.5$, one element through the film thickness was used (Fig. 7). For beam geometries whose substrate was significantly thicker than the first film ($R_{hl} \leq 0.5$), a variable element size through thickness was applied as shown in Fig. 7 to avoid the alteration of the frequency values. This mesh principle takes into account the effect of abrupt change in the size of the element at the film/substrate interface avoiding the cutoffs of the propagated waves that disturb the solution [56]. The resonant frequencies of the composite beam were extracted using the ABAQUS\Implicit Lanczos eigensolver. These configurations were chosen as a reference to validate the analytical models presented in section 2.

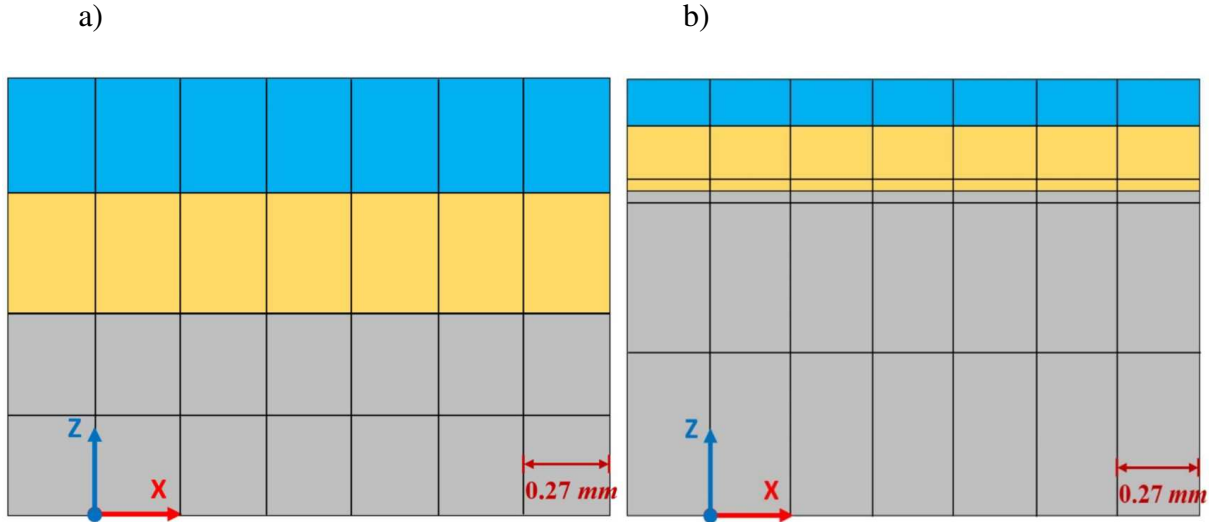


Fig. 7. Cross-section of FEM with the meshing configuration: a) $R_{hl} > 0.5$, b) $R_{hl} \leq 0.5$.

5. Modal analysis

A parametric comparison of the analytical models with the finite element model (FEM) was done with a combination of different Young's modulus and density ratios. The following values represent different configurations chosen to operate at the extreme border where the former models remain invalid [11, 22, 26].

For a bilayer beam, the evolution of the frequency ratio R_{fl} as a function of the thickness, density and Young's modulus ratios, is represented in Fig. 8 with the thickness ratio R_{hl} varying from 0 to 1. The ratios were chosen to cover a large range of materials used for surface coatings. A good agreement can be noted between the developed model (Dev-CLBT), Pautrot's model (Eq. (11)) and the FEM, for any R_{hl} , R_{El} and $R_{\rho l}$ ratios. The good reliability of Pautrot's model has already been shown in our previous paper [24]. As can be seen, the good agreement of Dev-CLBT model shows that the influence of symmetry becomes negligible when taking into account the shift of the neutral axis after the deposition of the first film. For thickness ratios < 0.1 , all models give approximately the same result. For thicker films ($R_{hl} > 0.1$), the discrepancies between the different models increase due to the different assumptions on which each model is based.

a) b)

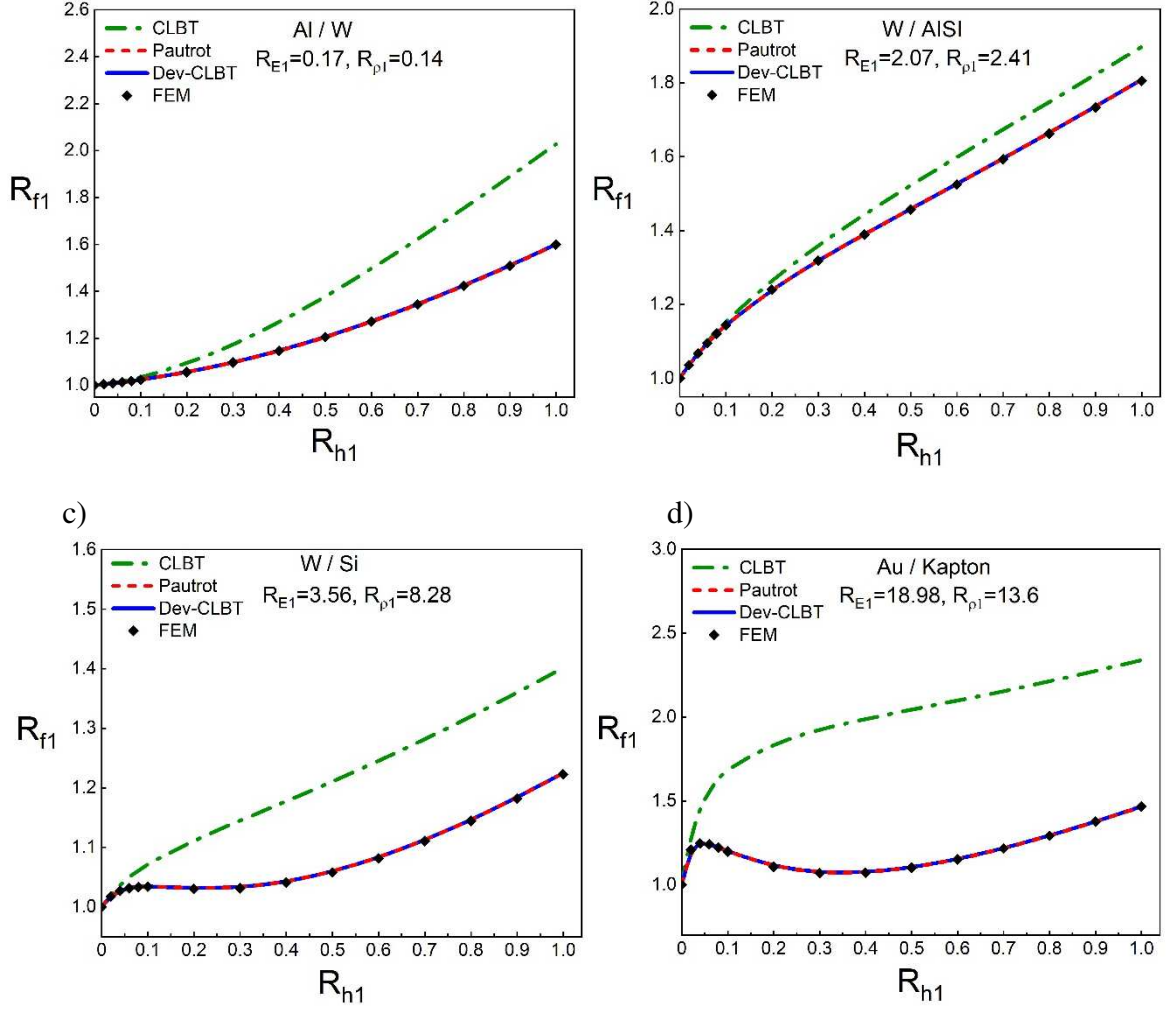


Fig. 8. Comparison between analytical and numerical models for bilayer isotropic beam (substrate + film) for different Young's moduli and density ratios: a) $R_{E1}=0.17, R_{\rho1}=0.14$, b) $R_{E1}=2.07, R_{\rho1}=2.41$, c) $R_{E1}=3.56, R_{\rho1}=8.28$, d) $R_{E1}=18.98, R_{\rho1}=13.6$.

For a three-layered beam (substrate + bilayer films), another comparison was done with different Young's modulus R_{E2} and density $R_{\rho2}$ ratios. Fig. 9 represents the evolution of the frequency ratio R_{f2} as a function of the thickness ratio R_{h2} that varies from 0 to 0.55 with two different values of R_{h1} equal to 0.004 and 0.1. A good agreement is noticed between the developed model (Dev-CLBT), the extended Pautrot's model (Ext-PM) (Eq. (36)) and the FEM. As for the case of a bilayer beam, we can clearly see the divergence of the CLBT model. This difference between the models increases with the thickness ratio R_{h2} .

a)

b)

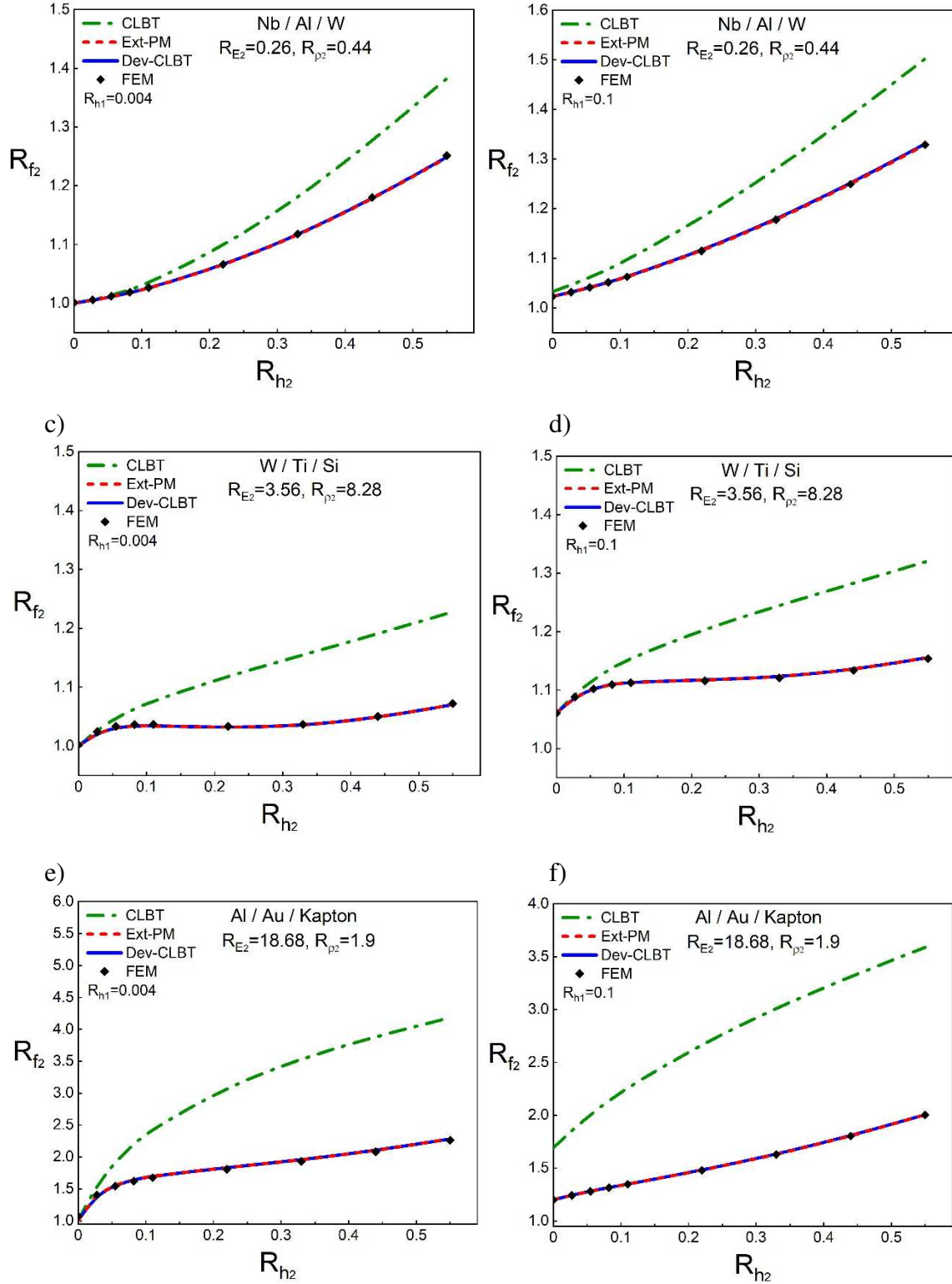


Fig. 9. Comparison between analytical and numerical models for a multilayer beam comprising three isotropic materials for different Young's moduli and density ratios: a) $R_{h1}=0.004, R_{E2}=0.26, R_{\rho2}=0.44$, b) $R_{h1}=0.1, R_{E2}=0.26, R_{\rho2}=0.44$, c) $R_{h1}=0.004, R_{E2}=3.56, R_{\rho2}=8.28$, d) $R_{h1}=0.1, R_{E2}=3.56, R_{\rho2}=8.28$, e) $R_{h1}=0.004, R_{E2}=18.68, R_{\rho2}=1.9$, f) $R_{h1}=0.1, R_{E2}=18.68, R_{\rho2}=1.9$.

The three models (Ext-PM, Dev-CLBT and FEM) predict very similar resonant frequencies for bilayer and three-layered beams. FEM is a numerical approach, which takes

into account the slenderness of the beam, and thus it can be considered as a reference to check analytical models. The difference between FEM and the two analytical models remains lower than 0.2 % in the range of the tested ratios (R_h , R_E and R_ρ), which is negligible. Consequently, the two models are validated and can be used for the prediction of the resonant frequencies. In the next sections, the two models will be used to determine the Young's modulus of each film in a multilayer beam.

6. Uncertainty analysis

The uncertainty analysis was performed using the ISO standard guidelines [45]. The uncertainty on a quantity x is defined as the standard uncertainty calculated $u(x)$ which is the standard deviation of the distribution of x values. In the present study, the quantitative values of the uncertainties of different sources related to the frequency measurements were imported from a previous work [24] where the experimental study was performed using the same IET set-up. Thus, other components of the uncertainty were calculated using the uncertainty propagation equation [57].

6.1. Frequency Uncertainty

A series of experimental measurements were performed to identify and estimate the different sources of uncertainty on the measured frequencies. The sources of uncertainty were determined on the IET [24] and they led to a significant influence on the frequency measurement. Table 4 represents the uncertainty of the first four resonance frequencies.

Table 4

Uncertainty on the first four resonance frequencies.

Uncertainty (Hz)			
Mode I	Mode II	Mode III	Mode IV
0.117	0.147	0.250	0.201

The global uncertainties of the resonant frequencies can be calculated from the following expression [24]:

$$u(f) = \sqrt{u_{pos}^2 + u_{align}^2 + u_{rep}^2 + u_{supp}^2} \quad (56)$$

Where u_{pos} , u_{align} , u_{rep} and u_{supp} are the uncertainties caused by the position of the microphone, the misalignment between the sample nodal lines and the supporting wires, the repeatability and the nature of the support, respectively.

It was found that the measurements are mostly affected by the nature of the support and the misalignment. The support and misalignment uncertainties present the highest contributions. This can be due to the approximate realization of the free-free condition.

6.2. Uncertainty on the substrate and coating Young's modulus

Using the equation of uncertainty propagation, the global uncertainty of the substrate Young's modulus was calculated by developing all the uncertainties that appear in Eqs. (4) and (5). The equation of uncertainty propagation is expressed by assuming that the covariance between the different parameters is null [45].

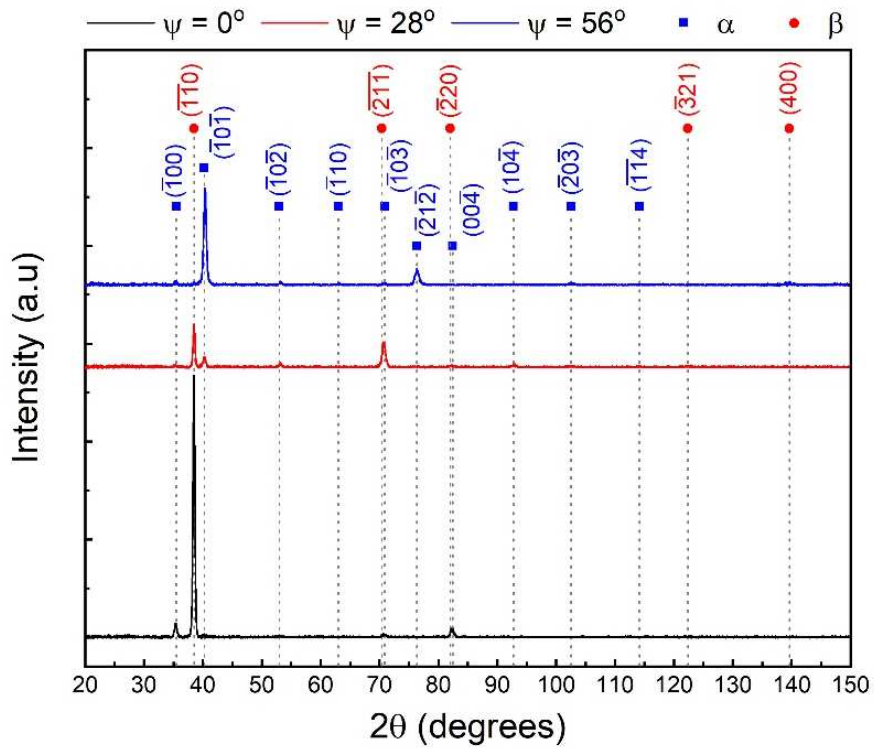
Using the dimensions uncertainties (Table 2) and the mass uncertainties (Table 3) discussed in section 3.2, the values of the uncertainty on the substrate density are calculated and presented in Table 3. Using the uncertainty of each quantity, the global uncertainty on the substrate Young's modulus was calculated. In a similar way, the uncertainty of the coating Young's modulus was calculated using the equation of uncertainty propagation for Ext-PM and Dev-CLBT. The uncertainty on Poisson's ratio was assumed negligible in the present calculation.

7. Results and discussion

7.1. Microstructure

Fig. 10 presents the X-ray diffraction patterns of the deposited titanium and niobium films. The presence of two phases: A body-centered cubic (bcc) metastable phase, known as β -Ti and a hexagonal closed packed (hcp) phase, known as α -Ti, can be clearly seen in the structure of the titanium film (Fig. 10a). These phases are classically observed on titanium as film [48] and as bulk material [58]. The presence of the metastable phase in the Ti film could be due to the deposition parameters [46, 59-61]. Contrariwise, the niobium film structure (Fig. 10b) exhibits a bcc single-phase α structure, similar to several studies on Nb thin films [49, 62-65].

a)



b)

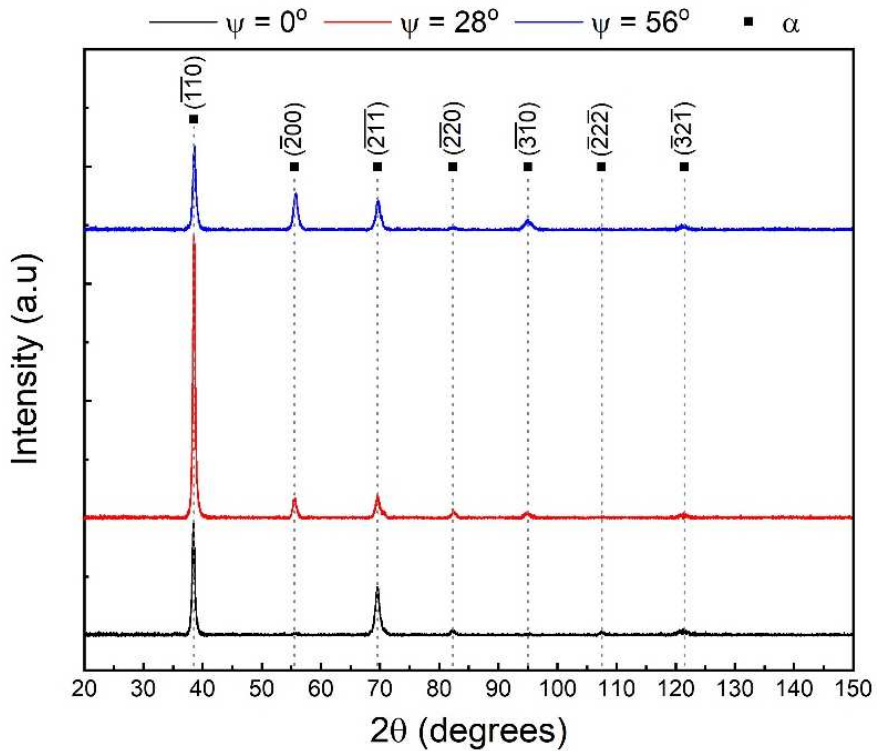


Fig. 10. X-ray diffraction patterns for different inclination angles: a) titanium film and b) niobium film.

7.2. Measurement of resonant frequencies in multilayers

Table 5 lists a summary of the resonance frequencies measured (average value) and the uncertainties for each layered system. The table presents the values measured on two

consecutive coatings of Ti and Nb deposited on AISI 316 (sample 1) and glass (sample 2) substrates under the same deposition parameters. An increase in $f^{(n)}$ is observed when each film is added. We can clearly see that the difference Δf in the measured frequencies before and after each deposition, is higher than their corresponding uncertainties, which gives the confidence to use them to determine the Young's modulus of each film. We can clearly see that the contribution (in %) on the measured frequency decreases by taking a higher mode which presents a higher frequency.

Table 5

Flexural resonance frequencies of samples measured by IET before and after deposition.

Mode shape	Sample	Flexural resonance frequency (Hz)			$\Delta f_1=f_1-f_0$ (Hz)	$\Delta f_2=f_2-f_1$ (Hz)	u(f)	
		Before deposition	After first deposition	After second deposition			(Hz)	%
I	1 (AISI 316)	534.54	537.12	537.90	2.58	0.78	0.117	0.02
	2 (Glass)	980.84	986.93	987.22	6.09	0.29	0.117	0.01
II	1	1481.98	1489.38	1491.70	7.40	2.32	0.147	0.01
	2	2712.05	2728.55	2729.43	16.50	0.88	0.147	5.4×10^{-3}
III	1	2907.49	2922.14	2925.87	14.65	3.73	0.250	8.6×10^{-3}
	2	5317.45	5351.86	5353.71	34.41	1.85	0.250	4.7×10^{-3}
IV	1	4807.60	4832.67	4839.57	25.07	6.90	0.201	4.2×10^{-3}
	2	8692.02	8743.18	8745.74	51.16	2.56	0.201	2.3×10^{-3}

7.3. Determination of Young's modulus in a three-layered beam

Table 6 gives the Young's moduli and uncertainties of different substrates obtained by IET using Eq. (5) for the fundamental frequency and Eq. (4) for the other frequency modes. The contribution of each uncertainty source is presented in Fig. 11 that corresponds to sample No. 1 (AISI 316). The measurements of the substrate's thickness and density present the main contributions on the prediction of the substrate Young's modulus E_0 . The global uncertainty and the various contributions are approximately the same for the first four frequency modes with percentages of 79 % and 20 % respectively, for the substrate thickness and density. Thus, a very precise and accurate measurement should be performed on the measurement of the thickness and the density of the substrate.

Table 6

Substrate Young's modulus and its uncertainties.

Mode shape	Sample	IET		
		E_0	u(E_0)	
		GPa	GPa	%
I	1 (AISI 316)	200.47	2.33	1.16
	2 (Glass)	69.90	1.25	1.78
II	1	202.70	2.36	1.16
	2	70.24	1.26	1.79
III	1	203.01	2.36	1.16
	2	70.26	1.26	1.79
IV	1	203.13	2.36	1.16

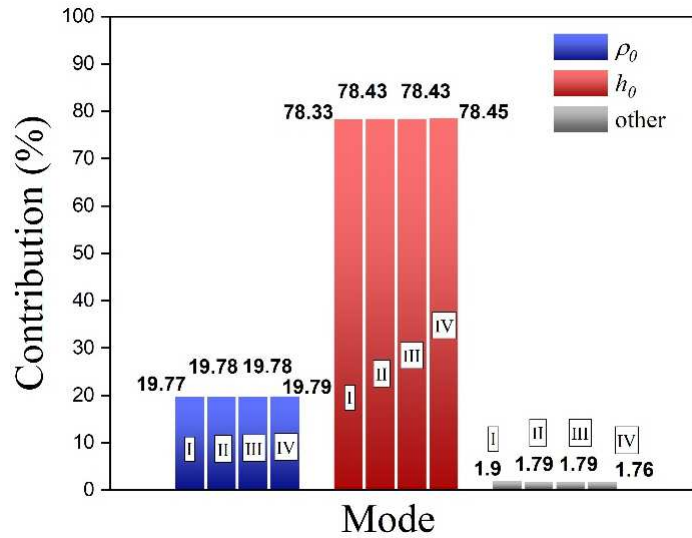


Fig. 11. Contribution of each uncertainty source (in %) on the AISI 316 substrate Young's modulus uncertainty.

In Tables 7 and 8, the Young's modulus and uncertainty of the deposited Ti and Nb films were obtained using Pautrot's, Dev-CLBT and Extended Pautrot's (Ext-PM) models. The Young's moduli are also obtained using nanoindentation. From Eq. (55) and the reduced modulus E_r measured, the corresponding Young's modulus and the uncertainty values were obtained. We can notice that the difference between the Young's moduli increases with the frequency mode. The difference between the modulus determined from the first frequency and the higher frequencies may be due to the effect of shear and inertia. They were taken into account in the frequency equation of the first mode (Eq. (5)) using the correction factor, which is not the case in the frequency equation of the other modes (Eq. (4)).

The Poisson's ratios used in CLBT and Dev-CLBT models for the glass and AISI substrates, were respectively 0.187 [38,68] and 0.265 [67]. For titanium and niobium films, the Poisson's ratios were respectively 0.36 [67] and 0.4 [66], which were taken from the literature for bulk behavior properties. Figs 12 and 13 present the frequency ratio as function of the ratio $R_{\nu_i} = \nu_i / \nu_0$. We can conclude from these figures that there is no significant influence of the Poisson ratio on the determination of the Young's modulus in flexural mode.

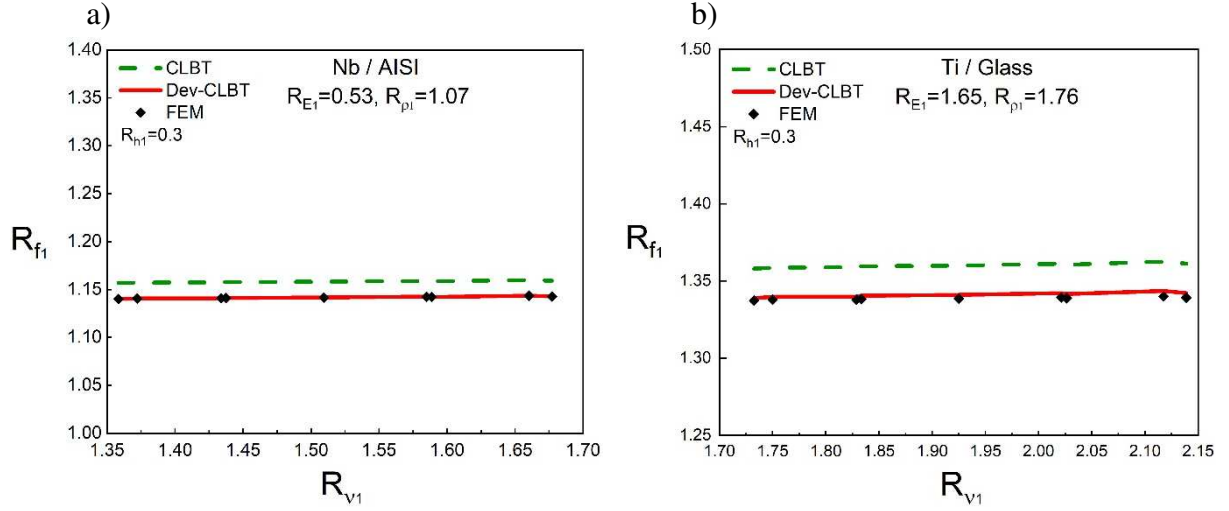


Fig. 12. Comparison between analytical and numerical models for bilayer isotropic beam (substrate + film) with $R_{h1}=0.3$ and for different Young's moduli, and density ratios: a) $R_{E1}=0.53$, $R_{\rho1}=1.07$, b) $R_{E1}=1.65$, $R_{\rho1}=1.76$.

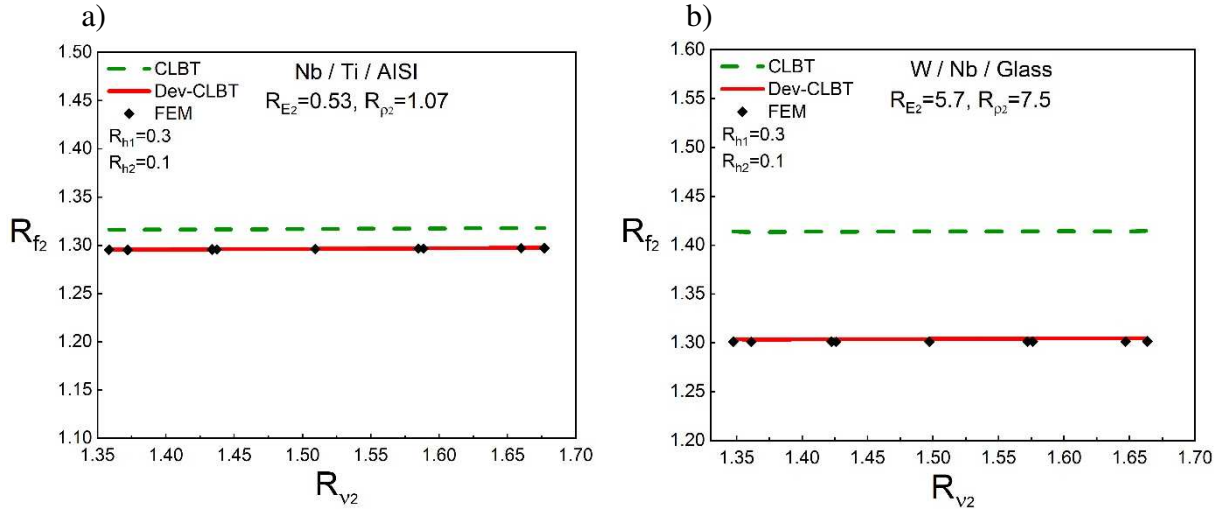


Fig. 13. Comparison between analytical and numerical models for a multilayer beam comprising three isotropic materials with $R_{h1}=0.3$, $R_{h2}=0.1$ and for different Young's moduli and density ratios: a) $R_{E2}=0.53$, $R_{\rho2}=1.07$, b) $R_{E2}=5.7$, $R_{\rho2}=7.5$.

For the first sample, the contribution on the Ti film Young's modulus is in the order of 4.6 GPa (4.4 %), 2.7 GPa (2.5 %), 2.5 GPa (2.3 %) and 2 GPa (1.8 %), respectively in mode I, II, III, and IV, approximately for the two models (Table 7). By passing from the first to the fourth mode, the resonant frequency of the system increases and its contribution decreases (Table 5). The frequency difference Δf increases by a factor of 10 from mode I to IV whereas the frequency contribution decreases by a factor of 5. Using the equation of uncertainty propagation for Pautrot's and Dev-CLBT models, the uncertainty of Ti film Young's modulus decreases. The same reasoning is applied to the second sample.

For a three-layered system, the uncertainty of the Nb film Young's modulus is in the order of 8 GPa (9 %), 5.4 GPa (5.8 %), 5 GPa (5.7 %) and 4 GPa (4.8 %) respectively in

mode I, II, III, IV with a slight difference between the two models, which was not the case for the bilayer beam. This difference appears starting from the second layer because of the difference in theory and the symmetry assumption of the laminated theory that can relatively disturb the results even if it was corrected by the shift of the neutral axis after deposition. The uncertainty of the second film Young's modulus is higher than that of the first film. This can be due to the layering where the cumulating effect of the uncertainties of the two precedent layers (substrate and the first coating) contributes to the second film Young's modulus.

Table 7

Young's modulus of the first film of Ti obtained by IET and NI.

Sample	Mode shape	First film (Ti)								
		Pautrot			Dev-CLBT			NI		
		E_1	$u(E_1)$		E_1	$u(E_1)$		E_1	$u(E_1)$	
		GPa	GPa	%	GPa	GPa	%	GPa	GPa	%
1 (AISI 316)	I	105.22	4.69	4.46	104.56	4.66	4.46	-	-	-
	II	108.74	2.72	2.5	108.07	2.75	2.54	-	-	-
	III	109.55	2.54	2.32	108.87	2.55	2.34	-	-	-
	IV	112.11	2.06	1.84	111.41	1.98	1.77	-	-	-
2 (Glass)	I	105.28	2.81	2.67	102.62	2.82	2.75	-	-	-
	II	104.54	2.37	2.27	101.9	2.22	2.18	107.26	2.89	2.7
	III	108.45	2.4	2.21	105.72	2.4	2.27	-	-	-
	IV	100.31	2.18	2.17	97.77	2.17	2.22	-	-	-

Table 8

Young's modulus of the second film of Nb obtained by IET and NI.

Sample	Mode shape	Second film (Nb)								
		Ext-PM			Dev-CLBT			NI		
		E_2	$u(E_2)$		E_2	$u(E_2)$		E_2	$u(E_2)$	
		GPa	GPa	%	GPa	GPa	%	GPa	GPa	%
1 (AISI 316)	I	89.53	8.31	9.28	88.21	7.68	8.71	-	-	-
	II	92.37	5.3	5.74	91.01	5.42	5.95	-	-	-
	III	87.74	5.01	5.71	86.45	4.91	5.68	-	-	-
	IV	90.42	4.38	4.84	89.09	4.09	4.59	-	-	-
2 (Glass)	I	82.64	5.89	7.13	79.35	5.76	7.26	-	-	-
	II	83.36	5.3	6.36	80.04	4.96	6.2	87.55	3.87	4.42
	III	83.78	5.37	6.41	80.44	4.9	6.09	-	-	-
	IV	81.11	4.98	6.14	77.89	4.52	5.8	-	-	-

Figs. 14 and 15 present the contribution of each uncertainty source on the uncertainty of the Ti and Nb film Young's moduli, respectively. They are calculated using the equation of uncertainty propagation for Ext-PM and Dev-CLBT models. As we can notice for both models, the measured density of the film, the substrate Young's modulus and the two frequencies represent a high percentage contribution, which are the first to be improved. The Ti film Young's modulus is added for the case of the three-layered system. The large contributions of the frequencies are related to the shift in the measured frequency before and after deposition.

Furthermore, we can clearly see that by increasing in mode, the contribution of the frequency on the film Young's modulus decreases progressively. Once the contribution of the frequency decreases, the contribution of the other parameters (E_0 , E_1 , ρ_1 , ρ_2 , etc.) increases. These parameters are included in the equation of uncertainty propagation.

Especially for a three-layered beam, the first film Young's modulus uncertainty presents a significant effect for the determination of the second film Young's modulus. It can reach 44 % and 27 % respectively for Ext-PM and Dev-CLBT models. The contribution on the Young's modulus of a thin film becomes higher with the addition of several films.

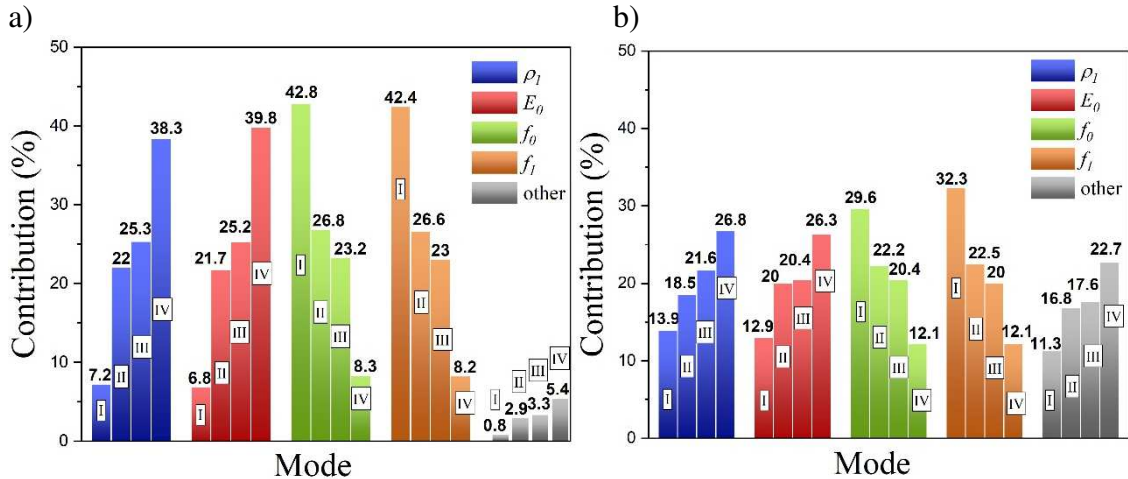


Fig. 14. Contribution of each uncertainty source (in %) on the first (Ti) film Young's modulus given by: a) Pautrot's model and b) Present model.

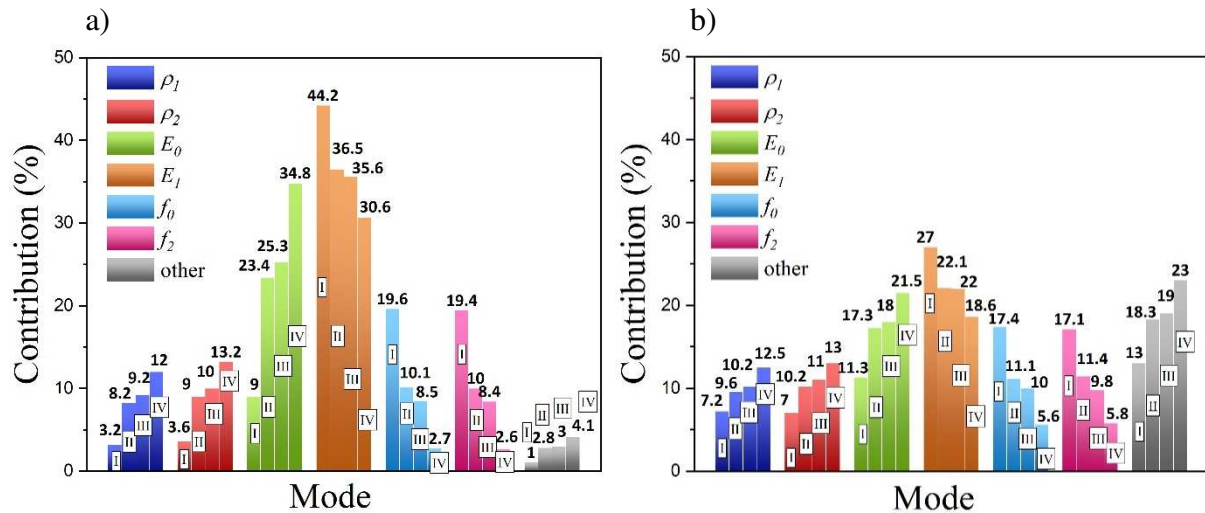


Fig. 15. Contribution of each uncertainty source (in %) on the second (Nb) film Young's modulus given by: a) Pautrot's model and b) Present model.

The measured Young's moduli of the substrates (Table 6) are coherent with the literature for AISI 316 [67] and glass substrates [21, 68]. The values of Young's moduli of the titanium film presented in Table 7 varied from 97 to 112 GPa. The values published in the literature are highly dispersed: the values found in the present work are consistent with some of them [69-71] and differ from some others [27, 29]. Differences can be explained by microstructural features such as phase proportions [72] or the presence of pores or by the

process itself like in reference [28] where ions are implanted into the crystalline structure during the deposition process.

The measured values of the niobium film Young's moduli varied in the range of 77 ~ 92 GPa (Table 8). These values are close to those reported in previous studies for a single layer of niobium [49, 62] and they are lower than those given in other studies [73]. This can also be due either to the presence of pores in the film or to the layering of different materials that can toggle the results and the prediction of the Young's modulus of individual thin film in a multilayer system. We can conclude that both models can be used to determine the Young's modulus of individual film in a multilayer system considering carefully the different uncertainty sources.

8. Conclusion

This work presents the development of new analytical models for the determination of the Young's moduli of thin films in multilayer structures by means of the Impulse Excitation Technique (IET). The proposed models are based on two different theories (FRCB and CLBT). The comparison with the finite element model was performed to validate the developed models and to check the validity range of the other models. It was shown that both Extended Pautrot's Model (Ext-PM) and the new one (Dev-CLBT) are recommended to determine the Young's moduli of thin films whatever the coating thickness and the elastic properties of the films and substrate.

Titanium (4.84 μm) and niobium (3.97 μm) thin films were sputtered on AISI 316, glass substrates and silicon wafers. The Young's moduli of the deposited Ti and Nb films were determined using Pautrot's and Dev-CLBT models. A good agreement was found between the obtained moduli and the values reported in the literature. However, some previous studies present values different from the measured ones. This difference might be due to the presence of pores in the two films. However, the presence of the metastable β -Ti phase in the titanium film can also alter the Young's modulus of the titanium film.

In the case of the studied material, the standard uncertainty on the substrate Young's modulus comes mainly from the uncertainty on its thickness (79 % of the total uncertainty) and density (20 % of the total uncertainty). The main uncertainty sources on the first and second films Young's moduli are the density of the two coatings, the Young's modulus of the substrate, the Young's modulus of the precedent coating, and the frequency before and after deposition.

The measurement uncertainty of the IET represents about 1.1 % for the substrate Young's modulus. The measurement uncertainties on the first and second films Young's moduli are calculated as a function of the frequency mode. By increasing the vibrational mode, the measurement uncertainty decreases from about 4.4 % to 1.8 % for the first film and from about 9 % to 4.8 % for the second film. The increase of the measurement uncertainties with the addition of another film may be due to the accumulation of uncertainties from the

successive films. The measured values of the film Young's modulus are lower than the bulk one; this might be due to the presence of pores in the as-deposited films.

We are currently extending our study to evaluate macroscopically the anisotropic behavior of thin films. Compared to Ext-PM, Dev-CLBT model can take into account the anisotropy and will allow us to develop the vibrational technique (IET) in order to determine the anisotropic moduli of coating in different directions.

Acknowledgments: The authors would like to thank the co-founders of CERA project: The European Union (Fond Européen de Développement Régional) and the Doctoral School in Science and Technologies at the Lebanese University (Réseau UT/INSA-UL).

References

- [1] A.S.H. Makhlof, Protective coatings for automotive, aerospace and military applications: current prospects and future trends, in: A.S.H. Makhlof (Ed.), *Handbook of Smart Coatings for Materials Protection*, Woodhead Publishing, Cambridge 2014, pp. 121–131.
- [2] X. Li, L. Chen, H. Liu, Z. Mi, C. Shi, L. Qiao, Atom doping in α -Fe₂O₃ thin films to prevent hydrogen permeation, *International Journal of Hydrogen Energy* 44 (2019) 3221–3229.
- [3] B.C. Sertel, N.A. Sonmez, M.D. Kaya, S. Ozcelik, Development of MgO: TiO₂ thin films for gas sensor applications, *Ceramics International*, 45 (3) (2019) 2917-2921.
- [4] J. Lee, J. Kim, B.J. Lee, J. Lee, H.W. Lee, M. Hong, H. Park, D.I. Shim, H.H. Cho, K. Kwon, Characterization of mesoporous silica thin films for application to thermal isolation layer, *Thin Solid Films*, 660 (2018) 715-719.
- [5] V. Tiron, C. Porosnicu, P. Dinca, I. Velicu, D. Cristea, D. Munteanu, Á. Révész, G. Stoian, C.P. Lungu, Beryllium thin films deposited by thermionic vacuum arc for nuclear applications, *Applied Surface Science*, 481 (2019) 327-336.
- [6] S. Achache, A. Alhoussein, S. Lamri, M. François, F. Sanchette, C. Pulgarin, J. Kiwi, S. Rtimi, Sputtered gum metal thin films showing bacterial inactivation and biocompatibility, *Colloids Surf. B: Biointerfaces* 146 (2016) 687–691.
- [7] X. Deng, N. Chawla, K.K. Chawla, M. Koopman, J.P. Chu, Mechanical behavior of multilayered nanoscale metal–ceramic composites, *Adv. Eng. Mater.* 7 (2005) 1099.
- [8] E.W. Williams, Magnetic thin films and multilayers in data storage applications, *Mater. Des.* 13 (1992) 115.
- [9] J. Romero, A. Lousa, E. Martinez, J. Esteve, Nanometric chromium/chromium carbide multilayers for tribological applications, *Surf. Coat. Technol.* 163–164 (2003) 392.
- [10] H. Ziegele, H.J. Scheibe, B. Schultrich, DLC and metallic nanometer multilayers deposited by laser arc discharge, *Surf. Coat. Technol.* 97 (1997) 385.
- [11] A. López-Puerto, A.I. Oliva, A vibrational approach to determine the elastic modulus of individual thin films in multilayers, *Thin Solid Films* 565 (2014) 228–236.
- [12] K. Nallamshetty, M.A. Angadi, R. Whiting, Young's modulus of Cu/Cr multilayer films, *Journal of Materials Science Letters* 12 (1993) 1333-1334.
- [13] M. Kubisztal, G. Haneczok, A. Chrobak, B. Rams, D. Miara, J. Rasek, Elastic properties of epoxy system coatings on aluminum substrate, *Surface and Coatings Technology* 204 (2009) 120-124.
- [14] V.D. Papachristos, C.N. Panagopoulos, L.W. Christoffersen, A. Markaki, Young's modulus, hardness and scratch adhesion of Ni-P-W multilayered alloy coatings produced by pulse plating, *Thin Solid Films* 396 (2001) 173-182.

- [15] C. Bellan, J. Dhers, Evaluation of Young modulus of CVD coatings by different techniques, *Thin Solid Films* 469–470 (2004) 214–220.
- [16] M. Radovic, E. Lara-Curzio, L. Riester, Comparison of different experimental techniques for determination of elastic properties of solids, *Mater. Sci. Eng. A* 368 (2004) 56–70.
- [17] Y. Tan, A. Shyam, W.B. Choi, E. Lara-Curzio, S. Sampath, Anisotropic elastic properties of thermal spray coatings determined via resonant ultrasound spectroscopy, *Acta Materialia* 58 (2010) 5305–5315.
- [18] M. Thomasová, P. Sedlák, H. Seiner, M. Janovská, M. Kabla, D. Shilo, M. Landa, Young's moduli of sputter-deposited NiTi films determined by resonant ultrasound spectroscopy: Austenite, R-phase, and martensite, *Scr. Mater.* 101 (2015) 24–27.
- [19] G. Pickett, Equations for computing elastic constants from flexural and torsional resonant frequencies of vibration of prisms and cylinders, *Am. Soc. Test. Mater., Proc.* 45 (1945) 846–865.
- [20] P. Gadaud, S. Pautrot, Application of the dynamical flexural resonance technique to industrial materials characterization, *Mater. Sci. Eng. A* 370 (2004) 422–426.
- [21] P. Gadaud, X. Milhet, S. Pautrot, Bulk and coated materials shear modulus determination by means of torsional resonant method, *Mater. Sci. Eng. A* 521–522 (2009) 303–306.
- [22] P. Mazot, S. Pautrot, Détermination du module d'Young de dépôts par flexion dynamique: Application aux systèmes bicouche et tricouche, *Ann. Chim. Sci. Mater.* 23 (1998) 821–827.
- [23] R. Whiting, M.A. Angadi, S. Tripathi, Evaluation of elastic moduli in thin-film substrate systems by the two-layer vibrating reed method, *Mater. Sci. Eng. B* 30 (1995) 35.
- [24] M.F. Slim, A. Alhussein, A. Billard, F. Sanchette, M. François, On the determination of Young's modulus of thin film with Impulse Excitation Technique, *J. Mater. Res.* 32 (3) (2017) 497–511.
- [25] J.A. Hoy Benítez, F. Avilés, F. Gamboa, R. Peón-Escalante, A.I. Oliva, Vibration modeling and testing of bilayer beams for determination of film elastic modulus, *Meas. Sci. Technol.* 23 (2012) 045605.
- [26] B.S. Berry, W.C. Pritchett, Vibrating reed internal friction apparatus for films and foils, *IBM J. Res. Dev.* 19 (1975) 334–343.
- [27] Y. Kim, Elastic modulus measurement of thin film using a dynamic method, *Journal of Electronic Materials*, 26 (1997) 1002–1008.
- [28] S. Peraud, S. Pautrot, P. Villechaise, P. Mazot, J. Mendez, Determination of Young's modulus by a resonant technique applied to two dynamically ion mixed thin films, *Thin Solid Films* 292 (1997) 55–60.
- [29] K.H. Cho, Y. Kim, Elastic modulus measurement of multilayer metallic thin films, *Journal of Materials Research* 14 (1999) 1996–2001.

- [30] S. Etienne, Z. Ayadi, M. Nivoit, J. Montagnon, Elastic modulus determination of a thin layer, *Mater. Sci. Eng. A* 370 (2004) 181–185.
- [31] X.N. Ying, L. Zhang, Y.H. Yuan, The mechanical spectra of deposited materials by a composite reed vibration method, *Physica B* 405 (2010) 2039.
- [32] T. Hanada, Y. Bessyo, N. Soga, Elastic constants of amorphous thin films in the systems $\text{SiO}_2\text{--Al}_2\text{O}_3$ and $\text{AlPO}_4\text{--Al}_2\text{O}_3$, *J. Non-Cryst. Solids* 113 (1989) 213.
- [33] N.J. Pagano, Exact solutions for rectangular bidirectional composites and sandwich plates, *J. Compos. Mater.* 4 (1970) 20.
- [34] P. Foraboschi, Three-layered plate: elasticity solution, *Compos. Part B* 60 (2014) 764.
- [35] A. Pagani, E. Carrera, M. Boscolo, J.R. Banerjee, Refined dynamic stiffness elements applied to free vibration analysis of generally laminated composite beams with arbitrary boundary conditions, *Compos. Struct.* 110 (2014) 305.
- [36] L. Dozio, Exact vibration solutions for cross-ply laminated plates with two opposite edges simply supported using refined theories of variable order, *J. Sound Vib.* 333 (2014) 2347.
- [37] S.S. Rao, *Vibration of Continuous Systems*, John Wiley & Sons, Inc. (2006) 713–720.
- [38] M.F. Slim, A. Alhussein, F. Sanchette, B. Guelorget, M. François, An enhanced formulation to determine the Young's and shear moduli of thin films by means of Impulse Excitation Technique, *Thin Solid Films* 631 (2017) 172–179.
- [39] M.F. Slim, A. Alhussein, M. François, Elasticity Constants of a Two-Phase Tungsten Thin Film, *ICEM proceedings*, MDPI (2018) doi: 10.3390/ICEM18-05272.
- [40] ASTM E1876, Standard Test Method for Dynamic Young's Modulus, Shear Modulus, and Poisson's Ratio by Impulse Excitation of Vibration, 2015.
- [41] J. Gere, *Mechanics of Materials*, Cengage Learning, 2003.
- [42] F. Gamboa, A. Lopez, F. Avilés, J.E. Corona, A.I. Oliva, A vibrating reed apparatus to measure the natural frequency of multilayered thin films, *Meas. Sci. Technol.* 27 (2016) 045002.
- [43] M.W. Hyer, *Stress Analysis of Fiber-Reinforced Composite Materials*, first ed. DEStech publications Inc., Lancaster, 2009.
- [44] Eric Walter. *Méthodes numériques et optimisation, un guide du consommateur*. 2015.
- [45] JCGM, 100:2008(E), *Evaluation of Measurement Data — Guide to the Expression of Uncertainty in Measurement*, 2008.
- [46] S. Achache, S. Lamri, A. Alhussein, A. Billard, M. François, F. Sanchette, Gum Metal thin films obtained by magnetron sputtering of a Ti-Nb-Zr-Ta target, *Mater. Sci. Eng. A* 673 (2016) 492–502.

- [47] J. Musil, Recent advances in magnetron sputtering technology, *Surf. Coat. Technol.* 100 (1998) 280–286.
- [48] G. Liu, Y. Yang, N. Jin, X. Luo, B. Huang, P. Li, Z. Kou, The structural characterizations of Ti-17 alloy films prepared by magnetron sputtering, *Applied Surface Science* 427 (2018) 774–781.
- [49] Z. Xu, L. Yate, Y. Qiu, W. Aperador, E. Coy, B. Jiang, S. Moya, G. Wang, H. Pan, Potential of niobium-based thin films as a protective and osteogenic coating for dental implants: The role of the nonmetal elements, *Materials Science and Engineering C* 96 (2019) 166–175.
- [50] H. Buckle, *L'essai de microdureté et ses applications*, Publications Scientifiques et Techniques du Ministère de l'Air, ISSN 0370-1999, 1960.
- [51] M.F. Doerner, W.D. Nix, A method for interpreting the data from depth-sensing indentation instruments, *J. Mater. Res.* 1 (4) (1986) 601–609.
- [52] W.C. Oliver, G.M. Pharr, An improved technique for determining hardness and elastic modulus using load and displacement sensing indentation experiments, *Journal of Materials Research* 7 (6) (1992).
- [53] W.C. Oliver, G.M. Pharr, Measurement of hardness and elastic modulus by instrumented indentation: advances in understanding and refinements to methodology, *Journal of Materials Research* 19 (1) (2004).
- [54] I.N. Sneddon, The relation between load and penetration in the axisymmetric Boussinesq problem for a punch of arbitrary profile, *Int. J. Eng. Sci.* 3 (1) (1965) 47–57.
- [55] *Abaqus Analysis User's Manual* (6.13).
- [56] R. Massabò, Cut-off frequencies and correction factors of equivalent single layer theories, *Procedia Engineering*, 199 (2017) 1466-1471.
- [57] C.K. Bullough, The determination of uncertainties in Dynamic Young's Modulus, Standards Measurement and Testing Project No. SMT4-CT97-2165 (2000).
- [58] S. Fréour, D. Gloaguen, M. François, A. Perronnet, R. Guillén, Determination of Single-Crystal Elasticity Constants in a cubic phase within a multiphase alloy - X-Ray Diffraction measurements and inverse scale transition modeling, *Journal of Applied Crystallography*, 38 (2005) 30-37.
- [59] V. Chawla, R. Jayaganthan, A.K. Chawla, Ramesh Chandra, Microstructural characterizations of magnetron sputtered Ti films on glass substrate, *Journal of Materials Processing Technology*, 209 (2009) 3444–3451.
- [60] V. Chawla, R. Jayaganthan, A.K. Chawla, Ramesh Chandra, Morphological study of magnetron sputtered Ti thin films on silicon substrate, *Materials Chemistry and Physics*, 111 (2008) 414–418.

- [61] H. Savaloni, A. Taherizadeh, A. Zندهnam, Residual stress and structural characteristics in Ti and Cu sputtered films on glass substrates at different substrate temperatures and film thickness. *Phys. B: Condens. Mat.*, 349 (2004) 44–55.
- [62] F. Seifried, H. Leiste, R. Schwaiger, S. Ulrich, H.J. Seifert, M. Stueber, Structure, morphology and selected mechanical properties of magnetron sputtered (Mo, Ta, Nb) thin films on NiTi shape memory alloys, *Surface and Coatings Technology*, 347 (2018) 379–389.
- [63] F. Gontad, A. Lorusso, M. Panareo, A.G. Monteduro, G. Maruccio, E. Broitman, A. Perrone, Nanomechanical and electrical properties of Nb thin films deposited on Pb substrates by pulsed laser deposition as a new concept photocathode for superconductor cavities, *Nucl. Instrum. Methods Phys. Res., Sect. A* 804 (2015) 132–136.
- [64] B. Okolo, P. Lamparter, U. Welzel, E.J. Mittemeijer, Stress, texture, and microstructure in niobium thin films sputter deposited onto amorphous substrates, *J. Appl. Phys.* 95 (2004) 466–476.
- [65] A. Goldmann, 2.11.7 Nb (Niobium) (Z=41), in: A. Goldmann (Ed.), *Noble Metals, Noble Metal Halides and Nonmagnetic Transition Metals*, Springer-Verlag, Berlin, Heidelberg (2003) 196–204.
- [66] J.-M. Zhang, Y. Zhang, K.-W. Xu, V. Ji, Young's modulus surface and Poisson's ratio curve for cubic metals, *J. Phys. Chem. Solids* 68 (2007) 503.
- [67] C.J. Smithells, *Smithells Metals Reference Book*, Butterworths, London, 1983.
- [68] A. Jämting, J. Bell, M. Swain, N. Schwarzer, Investigation of the elastic modulus of thin films using simple biaxial bending techniques, *Thin Solid Films* 308 (1997) 304–309.
- [69] T. Tsuchiya, M. Hirata, N. Chiba, Young's modulus, fracture strain, and tensile strength of sputtered titanium thin films, *Thin Solid Films* 484 (2005) 245–250.
- [70] M. Chinmulgund, R.B. Inturi, J.A. Barnard, Effect of Ar gas pressure on growth, structure, and mechanical properties of sputtered Ti, Al, TiAl, and Ti₃Al films, *Thin Solid Films*, 270 (1995) 260–263.
- [71] A.V. Verkhovtsev, A.V. Yakubovich, G.B. Sushko, M. Hanauske, A.V. Solov'yov, Molecular dynamics simulations of the nanoindentation process of titanium crystal, *Computational Materials Science*, 76 (2013) 20–26.
- [72] M.F. Slim, A. Alhussein, E. Zgheib, M. François, Determination of single-crystal elasticity constants of the beta phase in a multiphase tungsten thin film using impulse excitation technique, X-ray diffraction and micro-mechanical modeling, *Acta Materialia*, 175 (2019) 348-360.
- [73] H. Czichos, B. Skrotzki, F.G. Simon, *Das Ingenieurwissen: Werkstoffe*, Springer Vieweg, Berlin, Heidelberg, 2014.

Figure Captions

Fig. 1. Schematic representation of a multilayer beam. a) Free configuration of a multilayer beam. b) The z-coordinates of each layer in a cross-sectional view.

Fig. 2. Schematic representation of the shift of the neutral axis: a) cross-sectional view, b) stress distribution in three-layer composite beam.

Fig. 3. Schematic view of a symmetrical laminated beam.

Fig. 4. Cross-sectional SEM image of the titanium and niobium films deposited on silicon substrate.

Fig. 5. The natural frequency of the substrate (AISI 316), one layer coated substrate (Ti/AISI 316) and the multilayer comprising three materials (Nb/Ti/AISI 316).

Fig. 6. Deformed flexural vibrating beam: a) mode I, b) mode II, c) mode III and d) mode IV. The colors indicate the vertical displacement (mm).

Fig. 7. Cross-section of FEM with the meshing configuration: a) $R_{h1} > 0.5$, b) $R_{h1} \leq 0.5$.

Fig. 8. Comparison between analytical and numerical models for bilayer isotropic beam (substrate + film) for different Young's moduli and density ratios: a) $R_{E1}=0.17$, $R_{\rho1}=0.14$, b) $R_{E1}=2.07$, $R_{\rho1}=2.41$, c) $R_{E1}=3.56$, $R_{\rho1}=8.28$, d) $R_{E1}=18.98$, $R_{\rho1}=13.6$.

Fig. 9. Comparison between analytical and numerical models for a multilayer beam comprising three isotropic materials for different Young's moduli and density ratios: a) $R_{h1}=0.004$, $R_{E2}=0.26$, $R_{\rho2}=0.44$, b) $R_{h1}=0.1$, $R_{E2}=0.26$, $R_{\rho2}=0.44$, c) $R_{h1}=0.004$, $R_{E2}=3.56$, $R_{\rho2}=8.28$, d) $R_{h1}=0.1$, $R_{E2}=3.56$, $R_{\rho2}=8.28$, e) $R_{h1}=0.004$, $R_{E2}=18.68$, $R_{\rho2}=1.9$, f) $R_{h1}=0.1$, $R_{E2}=18.68$, $R_{\rho2}=1.9$.

Fig. 10. X-ray diffraction patterns for different inclination angles: a) titanium film and b) niobium film.

Fig. 11. Contribution of each uncertainty source (in %) on the AISI 316 substrate Young's modulus uncertainty.

Fig. 12. Comparison between analytical and numerical models for bilayer isotropic beam (substrate + film) with $R_{h1}=0.3$ and for different Young's moduli, and density ratios: a) $R_{E1}=0.53$, $R_{\rho1}=1.07$, b) $R_{E1}=1.65$, $R_{\rho1}=1.76$.

Fig. 13. Comparison between analytical and numerical models for a multilayer beam comprising three isotropic materials with $R_{h1}=0.3$, $R_{h2}=0.1$ and for different Young's moduli and density ratios: a) $R_{E2}=0.53$, $R_{\rho2}=1.07$, b) $R_{E2}=5.7$, $R_{\rho2}=7.5$.

Fig. 14. Contribution of each uncertainty source (in %) on the first (Ti) film Young's modulus given by: a) Pautrot's model and b) Present model.

Fig. 15. Contribution of each uncertainty source (in %) on the second (Nb) film Young's modulus given by: a) Pautrot's model and b) Present model.

Table Captions

Table 1

Summary of the analytical models.

Table 2

Average dimensions and measurement uncertainty.

Table 3

Mass and density with the measurement uncertainty.

Table 4

Uncertainty on the first four resonance frequencies.

Table 5

Flexural resonance frequencies of samples measured by IET before and after deposition.

Table 6

Substrate Young's modulus and its uncertainties.

Table 7

Young's modulus of the first film of Ti obtained by IET and NI.

Table 8

Young's modulus of the second film of Nb obtained by IET and NI.